

## Self-consistent Treatment of Copolymers with Arbitrary Sequences

YU.A. KUZNETSOV (\*), E.G. TIMOSHENKO(\*\*)

*Department of Chemistry, University College Dublin, Belfield, Dublin 4, Ireland*

### Summary. —

Using the Gaussian *Ansatz* for the monomer–monomer correlation functions we derive a set of the self-consistent equations for determination of the conformational state in the bead–and–spring copolymer model. The latter is based on the Edwards type effective free energy functional with arbitrary two–body interaction matrix. The rate of conformational changes in kinetics may be expressed via the instantaneous gradients of the variational free energy functional in the space of the averaged dynamical variables. We study the equilibrium and kinetics for some periodic and random aperiodic amphiphilic sequences in infinitely diluted solution. Typical equilibrium phase diagrams are elucidated and the conformational structure of different states is discussed. The kinetics of compaction of an amphiphilic copolymer to the globular state proceeds through formation of locally frustrated non–equilibrium structures. This leads to a rather complicated multistep kinetic process. We observe that even a small modification in the primary sequence of a copolymer may significantly change its kinetic folding properties.

PACS 36.20.-r – Macromolecules and polymer molecules.

PACS 64.60.My – Metastable phases.

PACS 64.70.Pf – Glass transitions.

PACS 01.30.Cc – Conference proceedings.

### 1. – Introduction

Conformational transitions of heteropolymers in dilute solutions attract special attention of theorists in recent years [1]. There is a significant body of works carried out on concentrated solutions, mixtures and blends of copolymers based on the density variables formulation [2]. The infinite dilution limit, for which such approaches cannot be used, is nevertheless very important for understanding the fundamental interactions of macromolecules not beset with the complications due to the aggregation phenomena. Apart from a purely academic interest, the single chain problem appears to be of paramount

---

(\*) E-mail: yuri@ucd.ie

(\*\*) E-mail: Edward.Timoshenko@ucd.ie, Web: <http://darkstar.ucd.ie>

importance for building up increasingly sophisticated models of *biopolymers* — the goal that seemed too remote only a decade ago. The progress in the modern biotechnology is often impeded by the inability to solve a few fundamental theoretical problems among which there is one grand challenge — given the primary sequence of macromolecule find its conformational structure at a given equilibrium, steady, or more interestingly, nonequilibrium state. The next part of the puzzle would be to find the relation between the conformational structure and biofunctionality of say a protein, but this sometimes can be explained by location of certain active sites on the surface of a protein globule.

The computational difficulties are clearly immense for even not so long protein chain of just about 60 amino acid residues. Therefore at the moment one hopes to develop merely some oversimplified models of heteropolymers abstracting from the accurate molecular level description. Such models are obtained by coarse-graining in a fashion normal for statistical mechanics by integrating out many of the local degrees of freedom. We hope to be able to deduce the mesostructure of a macromolecule and to obtain many of the important observables. The approach that we employ here is in its essence a nonequilibrium extension of the Gibbs–Bogoliubov variational principle. The main strength of the Gaussian self-consistent (GSC) method, which we [3, 4, 5] and others [6] were developing first for the simple homopolymer and in Ref. [7] we have brought to the most general form capable of describing copolymers, is in that it produces the complete set of mean squared distances between pairs of monomers and thus the conformational structure.

In this work we do not concentrate on the formal derivation of the GSC equations. This is presented in some detail in Ref. [7]. First, we shall introduce a crucially important modification to the model itself by adding a new so-called self-interaction term. We prove that without this regularising term the theory is plagued with divergences if at least one second virial coefficient is negative. We show that although the new term is seemingly negligible for long chain lengths, and indeed is not required for the coil, it does in fact the trick of correcting the structure of the dense globular state. In the rest of the work we carry out extensive study of the equilibrium properties and the folding kinetics for a number of examples of heteropolymer sequences. We also discuss how the spin glass behaviour arises for sufficiently random copolymer sequences.

## 2. – The Model and the GSC Equations

The main variables in the coarse-grained description of the polymer chain [8, 9, 10] are the spatial monomer coordinates  $\mathbf{X}_n$ , where  $n$  is the monomer number. The solvent molecules are excluded from the consideration by integrating out their degrees of freedom from the path integral representation for the partition function. The resulting monomer interactions are represented by the effective free energy functional (EFEF),

$$(1) \quad H = \frac{k_B T}{2l^2} \sum_n (\mathbf{X}_n - \mathbf{X}_{n-1})^2 + \sum_{J=2}^{\infty} \sum_{\{n\}} u_{\{n\}}^{(J)} \prod_{i=1}^{J-1} \delta(\mathbf{X}_{n_{i+1}} - \mathbf{X}_{n_i}),$$

where for heteropolymers  $u_{\{n\}}^{(J)}$  are in principle allowed to have any dependence on the site indices  $\{n\} \equiv \{n_1, \dots, n_J\}$ . The first term in Eq. (1) describes the connectivity of the chain with  $l$  called the statistical segment length. There are also volume interactions represented by the virial-type expansion [9, 10] in Eq. (1). They reflect the hard-core repulsion, the weak attraction between monomers and the effective interaction mediated by the solvent–monomer couplings.

Here we consider the following choice of site-dependent second virial coefficients in Eq. (1),

$$(2) \quad u_{nn'}^{(2)} = \bar{u}^{(2)} + \Delta \frac{\sigma_n + \sigma_{n'}}{2},$$

and  $u_{\{n\}}^{(J)} = u^{(J)}$  for  $J > 2$ . This corresponds to the case of amphiphilic heteropolymers, for which monomers differ only in the monomer-solvent coupling constants. The *mean second virial coefficient*,  $\bar{u}^{(2)}$ , is associated with the quality of the solvent and the parameter  $\Delta$  is called the *degree of amphiphilicity* of the chain. The set  $\{\sigma_n\}$  expresses the chemical composition, or the *primary sequence* of a heteropolymer. Here we consider the case when variables  $\sigma_n$  can take only three values:  $-1, 1$  and  $0$  corresponding to hydrophobic 'a', hydrophilic 'b' and "neutral" 'c' monomers respectively.

It is assumed that the long timescale evolution of the conformational state is well represented by the Langevin equation, which upon neglecting the hydrodynamics may be written as,

$$(3) \quad \zeta_b \frac{d}{dt} \mathbf{X}_n = -\frac{\partial H}{\partial \mathbf{X}_n} + \boldsymbol{\eta}_n(t),$$

where  $\zeta_b$  is the "bare" friction constant per monomer and the Gaussian noise,  $\boldsymbol{\eta}_n$ , is characterised by the second momentum,

$$(4) \quad \langle \eta_n^\alpha(t) \eta_{n'}^{\alpha'}(t') \rangle = 2k_B T \zeta_b \delta^{\alpha, \alpha'} \delta_{n, n'} \delta(t - t'),$$

where the Greek indices denote the spatial components of 3-d vectors.

The main idea of the Gaussian self-consistent method is to choose the trial Hamiltonian,  $H_0$ , as a most generic quadratic form, with matrix coefficients depending on time,

$$(5) \quad H_0(t) = \frac{1}{2} \sum_{nn'} V_{nn'}(t) \mathbf{X}_n(t) \mathbf{X}_{n'}(t).$$

This corresponds to the Gaussian distribution of the inter-monomer distances,  $(\mathbf{X}_m - \mathbf{X}_{m'})^2$ . Thus, the two-body monomer-monomer correlation function, that is the probability density to find the monomer  $m'$  at the distance  $r$  from the monomer  $m$ , will be given by,

$$(6) \quad h_{mm'}^{(2)}(\mathbf{r}; t) \equiv \langle \delta(\mathbf{r} - \mathbf{X}_m + \mathbf{X}_{m'}) \rangle = \frac{1}{(2\pi D_{mm'}(t))^{3/2}} \exp\left(-\frac{r^2}{2D_{mm'}(t)}\right).$$

Here  $D_{mm'}$  is the matrix of the mean squared distances between monomers,

$$(7) \quad D_{m m'}(t) \equiv \frac{1}{3} \langle (\mathbf{X}_m(t) - \mathbf{X}_{m'}(t))^2 \rangle.$$

Obviously, choosing Eq. (5) as the trial Hamiltonian is equivalent to replacing the non-linear Langevin equation (3) by a linear stochastic ensemble,

$$(8) \quad \zeta_b \frac{d}{dt} \mathbf{X}_n = -\sum_{n'} V_{nn'}(t) \mathbf{X}_{n'} + \boldsymbol{\eta}_n(t).$$

The time-dependent coefficients are chosen at each moment in time according to the criterion,

$$(9) \quad \left\langle \mathbf{X}_n \frac{\partial H}{\partial \mathbf{X}_{n'}} \right\rangle_0 = \left\langle \mathbf{X}_n \frac{\partial H_0}{\partial \mathbf{X}_{n'}} \right\rangle_0,$$

where  $\langle \dots \rangle_0$  denotes the averaging over the trial ensemble. At equilibrium these equations become exactly the extrema conditions for the trial free energy in the Gibbs–Bogoliubov variational principle based on minimising the variational free energy,  $\mathcal{A} = -k_B T \log \text{Tr} \exp(-H_0/k_B T) + \langle H - H_0 \rangle_0$ , with respect to  $V_{nn'}$ .

For details of calculations we refer the reader to Refs. [5, 7]. Here we present the final form of the kinetic GSC equations which describe the time evolution of the mean squared distances between monomers (7). It turns out that the equations can be written in terms of instantaneous gradients of the variational free energy,  $\mathcal{A} = \mathcal{E} - T\mathcal{S}$ ,

$$(10) \quad \frac{\zeta_b}{2} \frac{d}{dt} D_{mm'}(t) = -\frac{2}{3} \sum_{m''} (D_{mm''}(t) - D_{m'm''}(t)) \left( \frac{\partial \mathcal{A}}{\partial D_{mm''}(t)} - \frac{\partial \mathcal{A}}{\partial D_{m'm''}(t)} \right).$$

The energetic and the entropic contributions in the free energy can be completely expressed in terms of the mean squared distances  $D_{mm'}(t)$ ,

$$(11) \quad \mathcal{E} = \frac{3k_B T}{2l^2} \sum_n D_{n \ n-1, n \ n-1} + \sum_{J=2}^{\infty} \sum_{\{n\}'} \frac{u_{\{n\}}^{(J)}}{(2\pi)^{3(J-1)/2}} (\det \Delta^{(J-1)})^{-3/2} + \mathcal{E}_{si},$$

$$(12) \quad \mathcal{S} = \frac{3}{2} k_B \log \det R^{(N-1)}, \quad R_{nn'} = \frac{1}{N^2} \sum_{mm'} D_{nm, n'm'},$$

where we have introduced the four-point correlation function and the matrix  $\Delta^{(J-1)}$ ,

$$(13) \quad D_{mm', nn'} \equiv \frac{1}{2} (D_{m'n} + D_{mn'} - D_{mn} - D_{m'n'}),$$

$$(14) \quad \Delta_{ij}^{(J-1)} \equiv D_{n_1 n_{i+1}, n_1 n_{j+1}}.$$

In Eq. (12) we have the determinant of the truncated matrix  $R^{(N-1)}$  to exclude the zero eigenvalue related to the translational invariance for the centre-of-mass of the system. In the second term in Eq. (11), which is responsible for the volume interactions, the summation is taken over not coinciding indices,  $n_1 \neq n_2 \neq \dots \neq n_J$ .

Before proceeding with further discussions of the GSC equations let us introduce some observables. These include the mean squared radius of gyration,

$$(15) \quad R_g^2 = \frac{1}{2N^2} \sum_{mm'} D_{mm'},$$

and the micro-phase separation (MPS) order parameter,

$$(16) \quad \Psi = \frac{1}{N^2 R_g^2} \sum_{mm'} \frac{\sigma_m + \sigma_{m'}}{2\Delta_\sigma} D_{mm'}, \quad (\Delta_\sigma)^2 = \frac{1}{N} \sum_m \sigma_m^2.$$

The MPS parameter describes the degree of correlation between matrices of the relative two-body interaction,  $(\sigma_m + \sigma_{m'})/2$ , and the mean squared distances,  $D_{mm'}$ .

### 3. – The Self–interaction Energy Term

The appearance of the last term in Eq. (11),  $\mathcal{E}_{si}$ , is somewhat more nontrivial. In fact, in the EFEF of the model (1) we have discarded terms with two or more coinciding indices in the three– and higher body contributions. These terms come formally from the virial–type expansion, but each of them gives a singular contribution to the mean energy (11). It turns out, however, that upon suppressing these terms there appear additional pathological solutions of the GSC equations with singular free energy if at least one element of the two–body interaction matrix,  $u_{mm'}^{(2)}$ , becomes negative. This is easy to see. Indeed, consider volume interactions of just three monomers under condition that the mean squared distances from monomers '0' and '1' to '2' are equal to each other,  $D_{0,2} = D_{1,2} = D$ . These interactions produce the mean energy contribution,

$$(17) \quad \mathcal{E}_3 = \frac{u_{0,2}^{(2)} + u_{1,2}^{(2)}}{(2\pi D)^{3/2}} + \frac{1}{(2\pi D_{0,1})^{3/2}} \left( u_{0,1}^{(2)} + \frac{6u^{(3)}(2\pi)^{-3/2}}{(D - D_{0,1}/4)^{3/2}} \right)$$

In the case when  $u_{0,1}^{(2)} < 0$  and monomer '2' is placed away from monomers '0' and '1',  $D > D_{0,1}/4 + (6u^{(3)}(2\pi)^{-3/2}/|u_{0,1}^{(2)}|)^{2/3}$ , obviously in the limit  $D_{0,1} \rightarrow 0$  the energy possesses a singular minimum,  $\mathcal{E}_3 \rightarrow -\infty$ . As for the free energy, the logarithmic divergence of the entropy could not change the situation, thus  $\mathcal{A} \rightarrow -\infty$  as well. One can show that the inclusion of more monomers in the chain or of higher than three–body interactions does not improve the situation, but produces more and more of such pathological solutions. The reason we have not discussed this problem in our previous considerations is that we have accounted for the additional symmetry properties of monomer–monomer distances, which come from the symmetry of the EFEF (1). For example, in the case of the ring homopolymer, due to the inverse symmetry [5], we assumed that for any indices  $m, m'$  the following mean squared distances are equal,  $D_{m,m'} = D_{m,2m-m'} = D_{2m'-m,m'}$ . This provides sufficient repulsion coming from three–body term to preclude pathological solutions.

Thus, in a more general case, where no symmetry properties could be assumed for an arbitrary sequence, the standard procedure of suppressing terms with coinciding indices is not satisfactory. Fortunately, it could be remedied by using another prescription — replacing the terms with coinciding indices by the so–called self–interaction terms. Here we propose the prescription for three–body interaction which is sufficient for our current purposes,

$$(18) \quad \mathcal{E}_{si}^{(3)} = c_3 u^{(3)} \sum_{m \neq m'} \left\langle \delta(\mathbf{X}_m - \mathbf{X}_{m'}) \right\rangle^2 = c_3 \hat{u}^{(3)} \sum_{m \neq m'} D_{mm'}^{-3},$$

where  $c_3 = 3$  is a combinatorial factor related to the three possible ways of having coinciding pairs of indices in a triple summation. Obviously, the higher negative power of  $D_{mm'}$  in (18) compared to the two–body term in (11) prevents one monomer from falling on another.

It would be interesting to consider the coefficient  $c_3$  in Eq. (18) as an independent parameter and to discuss how the inclusion of this term would change the equilibrium and kinetics for the ring homopolymer [11]. Note that for the ring homopolymer we can reduce the number of independent elements in the matrix of mean squared distances,  $D_{mm'}$ , by the factor of  $N$ , since due to the translational symmetry,  $D_{m,m'} = D_{m+k,m'+k}$

for any  $k$  and  $m, m'$ . This symmetry allows us to reduce significantly the computational requirements.

In the good solvent regime,  $u^{(2)} > u^{(3)} > 0$ , we find no substantial change caused by the self-interaction term (18). The deviations in the mean squared distances and in the squared radius of gyration typically are less than 1% even for short chains. This is only natural. In this regime this term is subdominant for long chains and can be neglected at all in the thermodynamic limit.

However, the size and the structure of the homopolymer globule, which exists in the region  $u^{(2)} < 0$ , can change significantly. In Fig. 1 we exhibit the diagram of globular states. One can see that actually two different globular states are possible, which we call the non-compact globule (as one can see from Table I this globular state possesses a higher value of  $R_g^2$ ) and the liquid-like globule. The former is the thermodynamically stable state at comparatively small  $c_3$ , whilst the latter exists at higher values of  $c_3$  and in the region of large  $u^{(2)}$ . For large negative  $u^{(2)}$  the transition between two globular states becomes discontinuous and the transition line goes nearly vertically at approximately  $c_3 \approx 1/2$ . However, the collapse transition from the extended polymer coil to the liquid-like globule remains second order. We found that this phase diagram is quite independent of the degree of polymerization, at least in the range we could study numerically,  $30 \leq N \leq 200$ . Thus, introducing of the term (18), which is subdominant for large values of  $N$  compared to other terms in (11), nevertheless dramatically changes the properties of the globular state even for very long chains.

Now let us compare the structure of the non-compact and the liquid-like globules. In Fig. 2 in the left-hand side we present the mean squared distances, which are symmetrical with respect to the line  $m = N/2$ , i.e.  $D_{0,|m-m'|} = D_{0,N-|m-m'|}$ , for values of  $c_3 = 0, 3$ . In the right-hand side of the figure we draw the same quantity obtained from Monte Carlo simulations for a ring chain of hard spheres with the Lennard-Jones attraction [15]. Since the parameters of excluded volume interactions in the model used for Monte Carlo simulations are expressed in different terms, only shape and scaling behaviour, but not the absolute values of each  $D_{mm'}$ , should be compared. We see a quite remarkable agreement here. This is a strong argument in favour of the liquid-like globule. Its mean squared distances have a typical saturation regime after comparatively small  $m$ . This is known to be true of the globule from Monte Carlo simulations and previous results from other methods [12]. The function,  $D_{0m}$  for the non-compact globule has much more convex shape which, in fact, reflects the effective monomer repulsion on large distances (see Eq. (17)). Also, from Table I we can see that the asymptotic scaling in the degree of polymerisation for the size of the liquid-like globule,  $R_g^2 \sim N^{2/3}$ , is reached starting from sufficiently small  $N$  in agreement with lattice Monte Carlo simulations [13], whilst from much larger  $N$  for the non-compact globule [4].

Now, let us turn our attention to the kinetics at the collapse transition, after an instantaneous change of the value of the second virial coefficient from a positive to a negative value, the latter corresponding to the globular equilibrium state. In Fig. 3 we exhibit the evolution of the mean squared radii of gyration after quenches to the liquid-like and the non-compact globule. We found that the early stage proceeds in a similar manner, while the middle or ‘‘coarsening’’ kinetic stage is somewhat slower for quenches to the liquid-like globule, but the final stages here are much faster. This can be seen from Tab. I, where we present the values of the total collapse time [14] and the final relaxation time,  $\tau_f$  for different sizes,  $N$ . The most striking thing here is that the effective exponent of the final relaxation time is much smaller than what we have earlier expected,  $\gamma_f = 5/3$  (see Ref. [3, 4]). This also shifts down the effective exponent of the ‘‘total’’

collapse time, since the latter is a cross-over between the exponent of the coarsening stage,  $\gamma_m = 2$ , which is unaffected by the self-interaction term, and the exponent of the final relaxation,  $\gamma_f$ . In principle, the final relaxation time and its exponent in the degree of polymerization can be determined without appealing to numerical solution of the kinetic GSC equations. From Ref. [3] we have,  $\tau_f \sim N\mathcal{F}_1$ , where  $\mathcal{F}_1$  is the first normal mode for the final equilibrium globular state,

$$(19) \quad \mathcal{F}_q = -\frac{1}{2N} \sum_m \cos \frac{2\pi qm}{N} D_{0m}.$$

A good approximation for the function  $D_{0m}$  in the liquid-like globule would be the following  $D_{0m}$  is linearly increasing function of  $m$  until some value  $D_{0m_1} = D$ , where the  $N$ -dependence is,  $D \sim m_1 \sim N^{2/3}$  and then it remains constant. This approximation can also be obtained from the Lifshitz theory [12]. Now one can see that  $\mathcal{F}_1 \sim N^{1/3}$  and, correspondingly,  $\gamma_f = 4/3$ , which is close to the value of the effective exponent in Tab. I. Thus, on the contrary to the coil state, for the liquid-like globule the first normal mode,  $\mathcal{F}_1$ , neither gives the main contribution to the mean squared radius of gyration, nor even has the same scaling law in the degree of polymerization,  $N$ .

Inclusion of the self-interaction term (18) also strongly affects the phase diagram and kinetic properties of rigid chains. We shall consider these questions in a separate work [15]. Such modifications are rather welcome and allows one to make the GSC method more accurate for the dense globular states, where its validity has been less established.

#### 4. – Equilibrium Properties of Copolymer Sequences

The GSC equations (10) have been studied numerically using the fifth order Runge-Kutta algorithm with adaptive time step [16]. In fact, for copolymer sequences, considered in the current work, the time step during numerical integrations of Eqs. (10) varies approximately 100 times. Thus, any integration scheme with fixed time step is rather unreliable here.

In studying the equilibrium we consider only stationary points of Eqs. (10), i.e. the limit  $t \rightarrow \infty$ . If for some set of interaction parameters,  $\bar{u}^{(2)}$  and  $\Delta$ , one obtains several stationary states, one should compare the values of the variational free energy,  $\mathcal{A}$ . The deepest minimum of the free energy corresponds to the thermodynamically stable state, the rest of the solutions to metastable states. Here we consider copolymers with the ring topology, though the current treatment may be easily extended for study of copolymers with any other topology just by changing the spring term in Eqs. (1, 11).

Typical phase diagrams in terms of the mean second virial coefficient,  $\bar{u}^{(2)}$ , and the amphiphilicity,  $\Delta$ , in Eq. (2) for some “random” and periodic sequences are presented in Figs. 4-6. In the region  $\bar{u}^{(2)} > 0$  and for small values of amphiphilicity,  $\Delta < 5$ , typical conformations of copolymers are akin to the homopolymer extended coil. By decreasing  $\bar{u}^{(2)}$  to the negative region the chain undergoes the continuous collapse transition, similarly to what we observed in Sec. 3. The collapse transition is characterised by a rapid fall of the radius of gyration,  $R_g^2$ , (15) and the change of the fractal dimension,  $\nu$  (see Tab. I).

The collapse transition for larger values of amphiphilicity turns out to be more complicated, and essentially dependent on the sequence. The globular state for large values of  $\Delta$  is different from the liquid-like globule. It is characterized by somewhat higher value of the radius of gyration and extremely large value of the MPS order parameter (16), thus

we call this state the MPS globule. The MPS globule is separated from the liquid-like one by a weak continuous transition (see Figs. 4-6). In the case of long blocks (Fig. 6) the collapse transition to the MPS globule becomes discontinuous (first-order-like). The spinodals I' and I'' designate the region where two distinct states corresponding to the coil and the MPS globule can be found. The depths of the free energy minima become exactly equal on the transition curve I in Fig. 6.

However, for a wide class of sequences, for example for aperiodic sequences in Figs. 4, 5, the phase diagram at large amphiphilicity,  $\Delta$ , is much more complicated. Starting from some value of  $\Delta$  in some intermediate region of  $\bar{u}^{(2)}$  there appear additional solutions corresponding to local minima of the free energy. The broad region where this could take place is bounded by the curves I' and II'' in Figs. 4, 5. With increasing  $\Delta$  the number of such solutions grows quickly. Significantly, in the region of the phase diagram, between curves I and II in Figs. 4, 5, some of these possess the lowest free energy value, thus being the thermodynamically stable state. Since the number of such solutions is rather high even for short sequences and their number grows quickly with the chain length, we do not attempt to draw all their boundaries of (meta)stability. We shall call them collectively as *frustrated phases*, explaining this terminology below.

Now let us compare the phase diagrams in Figs. 4 and 5, the latter corresponding to the sequence twice longer than the former. An interesting observation is that the region between spinodals I' and II'', designating where the frustrated phases can exist, expands dramatically with increasing chain length. The same concerns the region of thermodynamically stable frustrated phases between curves I and II. More exactly, these regions expand downwards and to the left, so that the position of curves I' and I change slightly with increasing  $N$ , whilst curves II and II'' depend significantly on the size of the system. For rather long chains we may expect that the regions of stability and metastability of the frustrated phases will continue to expand downwards and to the left, so that the lines II and II'' will become nearly vertical, displacing the region of stable MPS globule. Probably, for most of long heteropolymer chains the MPS globule does not exist as thermodynamically stable state, becoming stable only for some special sequences. Unfortunately, we can not proceed with numerical solution for much larger system sizes,  $N$ , since the calculational expenses grow in  $N$  as  $N^3$  per iteration and also the total number of frustrated states becomes huge for large system sizes. This diversity and a special foliating structure of various branches leads in the thermodynamic limit to what is known as a spin glass frozen phase [17] of random copolymers.

Let us consider the conformational structure of the frustrated states for the copolymer consisting of repeating 'ab' blocks. The phase diagram of this sequence also exhibits the thermodynamically stable frustrated phases [7] starting from approximately  $N = 28$ . In Figs. 7 and 8 we present the dependence of the observables in (15, 16) at a quasistatic change of the mean second virial coefficient,  $\bar{u}^{(2)}$ , from the coil state to the MPS globule and back. From these pictures one can see in the intermediate region only a few (seven to be precise) of all possible frustrated phases. The values of the radius of gyration and the MPS order parameter are intermediate for these solutions, lying between those of the coil and the MPS globule. In this sense, we can call them non-fully compacted and misfolded states.

In the series of pictures in Fig. 9 we present the matrix of mean squared distances,  $D_{mm'}$ , for the copolymer, consisting of 'ab' blocks at some values of the mean second virial coefficient,  $\bar{u}^{(2)}$ . The set of  $D_{mm'}$  in the GSC method completely determines the conformational structure of any, equilibrium or kinetic, state. For positive  $\bar{u}^{(2)}$  (see Fig. 9a) the mean squared distances possess the structure typical for the extended coil.



The elements of the matrix,  $D_{mm'}$ , increase monotonically on moving away from its diagonals towards the distance of half-ring along the chain. Thus, the  $D_{mm'}$  matrix may be approximated here by a monotonically increasing function of the chain distance,  $|m - m'|$ . Decreasing the mean second virial coefficient,  $\bar{u}^{(2)}$ , causes the copolymer to pass through frustrated states, in Figs. 9b-9d, finally reaching the MPS globule state (see Fig. 9e). The characteristic feature of the  $D_{mm'}$  matrix in a frustrated state is that it possesses some number of monomer groups having smaller distances between each other than between monomers from other groups. Clearly, such a group represents a cluster of monomers, so that here the copolymer chain forms a set of clusters (approximately 8 clusters in Fig. 9b, 4 clusters in Fig. 9c and 2 clusters in Fig. 9d), each consisting of monomers nearest along the chain.

The internal structure of each cluster is similar to the structure of the final MPS globule. For the simplest copolymer sequence presented here, the  $D_{mm'}$  matrix away from the diagonal can be divided into sub-matrices of the size  $2 \times 2$  (see top of the Fig. 9e), each of which possesses approximately the same structure: small values in the upper left corner correspond to the mean squared distances between hydrophobic monomers; large values in the lower right corner, which are the mean squared distances between hydrophilic monomers; and off-diagonal elements are nearly equal and correspond to the distances between different species. Thus, for the MPS globule, such structure of the  $D_{mm'}$  matrix reflects the structure of the two-body interaction matrix,  $u_{mm'}^{(2)}$ . Obviously, the higher correlation between these two matrices is manifested in the higher value of the MPS order parameter. For another, more complicated, sequences the  $D_{mm'}$  matrix in the MPS globular state has a different structure, but still it resembles in some way the interaction matrix,  $u_{mm'}^{(2)}$  away from the diagonal, being distorted by the spring interactions in the elements close to the diagonal. Note that for the liquid-like globule the pattern of the  $D_{mm'}$  matrix looks sufficiently trivial. Namely, it has narrow band of dark color along the main diagonal with its intensity quickly decreasing, as one can see from Fig. 9f.

From Fig. 9 one can see that the interaction symmetries imposed by the EFEF (1) are spontaneously broken in the region of the phase diagram corresponding to the frustrated phases. Obviously, in our case the number of possible ways to break the symmetry is enormously huge and moreover it grows exponentially with increasing system size. Despite the kinematic symmetries are not present for arbitrary sequences, the structure of the phase diagram (see Figs. 4, 5) and behaviour of main observables remain very similar. It is the particular structure of  $D_{mm'}$  matrix, number and the shape of boundaries of frustrated phases that are quite sensitive to the sequence. The symmetry that may be broken in this case has a subtler meaning and may be expressed in terms of the replica formalism [17]. Consider, for example, two nearly identical blocks with nearly identical surroundings. In the coil and the MPS globular states one should expect the conformational matrices of these blocks to be nearly equal to each other. On the contrary, the small difference in the interactions in the region of frustrated phases may lead to a huge difference in the conformations. Thus, it is by no means surprising that the replica symmetry breaking in the case of periodic systems takes such an explicit manifestation in the breaking of the block translational symmetry.

An important point here is that the frustrated phases become dominant in an intermediate region of the phase diagram not due to a low mean energy, but mostly due to a higher entropy. The MPS globule is entropically unfavourable there because the overall shrinking force is insufficiently strong. Also, in the regime of nearly compensating repul-

sion and attraction between monomers it is more preferable to achieve phase separation on a smaller, than the globular, scale by forming clusters.

## 5. – Folding Kinetics

Here we shall consider the time evolution of the conformational state of a copolymer away from the initial equilibrium after it has been subjected to an instantaneous temperature jump that causes the two-body interaction parameters in Eq. (2),  $\bar{u}^{(2)}$  and  $\Delta$ , to change. The composition of copolymer  $\{\sigma\}$  and the rest of parameters remain the same and do not change with time. We are interested in quenches from the homopolymer coil, where all monomers are equally hydrophilic ( $\bar{u}^{(2)} > 0$  and  $\Delta = 0$ ), to the region of parameters corresponding to the MPS globular state, so that the 'a' species became strongly hydrophobic and the 'b' species remained nearly neutral ( $\bar{u}^{(2)} \ll 0$  and  $\Delta \approx |\bar{u}^{(2)}|$ ). Here we consider some binary copolymer systems, consisting of the same number of 'a' and 'b' monomers and of the same size,  $N = 50$ , and quench, ( $\bar{u}^{(2)} = 15$ ,  $\Delta = 0$ )  $\rightarrow$  ( $\bar{u}^{(2)} = -35$ ,  $\Delta = 30$ ).

Let us first discuss the general features of the kinetics of the copolymer folding. The time evolution of the mean squared radius of gyration,  $R_g^2(t)$ , the MPS order parameter,  $\Psi(t)$ , and the instantaneous free energy,  $\mathcal{A}(t)$ , is presented in Figs. 10, 11. Here lines A correspond to the homopolymer and serve for reference purposes. In the case of the homopolymer one can see that  $R_g^2$  and  $\mathcal{A}$  decrease monotonically to their equilibrium values corresponding to the liquid-like globule state, while  $\Psi$  remains identically zero. As for the copolymer kinetics, the first observation consists in that it proceeds much slower than for the homopolymer. For example, for the simplest copolymer sequence, '(ba)<sub>25</sub>', the total collapse time [14] is more than 3 times longer than that of the homopolymer, other copolymer sequences collapsing even longer. The total collapse time also seems to be quite sensitive to the copolymer sequence. Since the micro-phase separation is one of the main factors in collapse of copolymers, the MPS order parameter,  $\Psi$ , grows in kinetics most of the time for all considered sequences, though rather nonmonotonically. Nevertheless, for some sequences it might be negative during some time in kinetics (see e.g. sequences E and F in Fig. 11b), something we never observed at equilibrium.

The evolution of the instantaneous free energy,  $\mathcal{A}(t)$ , depicted in Figs. 10c, 11c, is most unusual. Typically it proceeds through multiple accelerations and decelerations. The flat regions of a staircase-like function correspond to temporary kinetic arrest of the system in transient nonequilibrium conformations, i.e. to transient trappings of various members of the ensemble in their local shallow energy minima. Since such minima are encountered at different moments in time for different members of the ensemble, their influence on the overall time evolution of averaged observables is manifested in a smooth characteristic slowing down. Note here that the number of steps in kinetics process hardly can be guessed from the given primary sequence. Typically, the kinetics for sequences with smaller number of blocks proceeds through smaller number of steps. For example, folding of the periodic sequence consisting of long blocks, '(b<sub>5</sub>a<sub>5</sub>)<sub>5</sub>' (see line E in Fig. 11c), proceeds through only one, though rather long, kinetically arrested step. However, for the aperiodic sequence of long blocks (line F in Fig. 11c) we can see at least six such steps, the third one being the longest in time.

Now let us consider the nonequilibrium conformations, given by the matrix of the mean squared distances between monomers,  $D_{mm'}$ . In Fig. 12 we exhibit the  $D_{mm'}$  matrix for '(ba)<sub>25</sub>' sequence at different times in the folding kinetics. We can see that kinetic process proceeds through formation of locally collapsed and phase-separated clusters.

The initial conformation is similar to Fig. 9a, then at time  $t = 3.6$  we can see approximately 10 clusters (Fig. 12a), at time  $t = 5.75$  — 6 clusters (Fig. 12b) and at  $t = 8.6$  — 4 clusters (Fig. 12c). During later evolution these four clusters approach each other since, as one can see from Fig. 12d, the inter-cluster distances are much smaller than in Fig. 12c. Finally, the clusters unify forming the MPS globule, the  $D_{mm'}$  matrix of which is quite similar to that presented in Fig. 9e. We should note here also that these nonequilibrium states do not possess the translational block symmetry, present for the system in the EFEF and the initial conditions. After some time in kinetics,  $t \approx 1$  this symmetry breaks down, and restores only during final kinetic stages at time moment  $t \approx 15$ .

However, the formal structure of the GSC kinetic equations (10) is such that they yield a symmetric solution at any moment in time if one proceeds from the symmetric initial condition. What we observe here is a spontaneous symmetry breaking in kinetics. Namely, at some moment in time the symmetric solution of the kinetic equations becomes unstable with respect to perturbations, whether of the initial condition, or of the interaction matrix,  $u_{nn'}^{(2)}$ . In the exact theory there are fluctuations that can transform between different spontaneously broken states in kinetics, thus destroying the unstable symmetric state. To describe such phenomena strictly in the framework of the Gaussian method, which presents an improved, but still a mean-field type of theory, we should include explicitly an infinitesimal symmetry breaking term  $\varepsilon_{nn'}$  to the two-body interaction matrix,  $u_{mm'}^{(2)}$ , and consider the limit of vanishing perturbation in the solution. In fact, in numerical integration such a regularisation procedure is not even necessary, since there is always an intrinsic perturbation due to computer round off and numerical integration errors. Thus, if the symmetry is favourable to be kinetically broken somewhere, numerically one obtains some spontaneously broken solutions there, rather than the unstable symmetric solution, unless the symmetry conditions have been imposed by hand. In fact, adding a rather small perturbation matrix,  $\varepsilon_{nn'}$ , changes the behaviour of the global observables, such as  $R_g^2$ ,  $\Psi$ ,  $\mathcal{A}$  and characteristic kinetic times rather insignificantly. However, what can be changed by including of a perturbation is the centers along the chain around which clusters form and grow.

Finally, let us discuss how the folding kinetics depends on the sequence. In series of pictures in Fig. 10 we present kinetic processes for the simplest copolymer consisting of 'ab' blocks (sequence B), and also for some sequences obtained by certain modifications in it. In the sequence denoted by C in Fig. 10 we have replaced ten short blocks by four of longer size. In the sequence D we have inserted only two hydrophobic and two hydrophilic fragments into the sequence, i.e. we have made only two permutations. For the former sequence the total kinetic time became approximately 1.7 times longer than that for the B sequence. The final values of the free energy for both sequences B and C are nearly the same, whilst the micro-phase separation is somewhat better for the modified sequence C, due to longer blocks. Thus, for that sequence the kinetic properties do not deteriorate very much, except that kinetic process takes essentially longer. However, the kinetic foldability of the D sequence is much more poor than for B and C sequences. In fact, here not only the kinetic process takes much longer, but the final state is different from the MPS globule. As one can see from Fig. 13 the final kinetic state for the D sequence consists of two clusters. These clusters are connected by two links, formed by nearly neutral fragments, 'b<sub>2</sub>'. Further collapse of this conformation is unfavourable due to the entropy and partial screening of hydrophobic monomers by nearly neutral species 'b'. Size of such misfolded state is larger and the MPS order parameter is approximately

twice smaller than what we could expect for the MPS globule. As we have already seen kinetics of sequences consisting of longer blocks is also quite sensitive to the sequence. Some modifications of the periodic sequence E in Fig. 11 to form aperiodic long blocks sequence, F, result in somewhat longer, but much more complicated, kinetic processes.

## 6. – Conclusion

In this paper we applied the extended GSC method to studying the equilibrium and kinetic phenomena of some particular amphiphilic heteropolymer sequences. First, we have revised the Gaussian theory to include the self-interaction term (18). Thus, the two-body term in our formalism describes the effective interactions between monomers, the self-interaction term is responsible for stability of the globular state, and the three-body interactions between distinct monomers provide the correct scaling of the size of the globule. The structure of the homopolymer globule is now in better agreement with the one obtained from other methods. We have found that the kinetic laws of the ring homopolymer do not change significantly due to introduction of the self-interaction term, except for the final relaxation time, which without hydrodynamic interaction scales with the degree of polymerization as,  $\tau_f \sim N^{4/3}$ .

We have obtained typical phase diagrams for heteropolymers consisting of short and long blocks. For sequences with rather frustrated interactions along the chain, apart from the coil, the liquid-like and the micro-phase separated globular states, we have discovered that in a wide intermediate region of the phase diagram there may be a large number of frustrated partially misfolded states. Some of such states, the number of which grows exponentially with the chain length, become the dominant thermodynamic state in rather narrow domains. We may conclude that the transition to these states for large systems corresponds to a glassy freezing transition.

For large amphiphilicity parameter collapse from the extended coil state to the MPS globule for a wide class of sequences proceeds at equilibrium through these frustrated phases. A typical copolymer conformation here is a set of micro-phase separated clusters. On approaching the MPS globule quasistatically the number of clusters decreases, reaching only one cluster in the final MPS globular state. A typical cluster size is determined by some characteristic range where the micro-phase separation may occur.

We have discovered that the region of meta- and thermodynamic stability of the frustrated phases expands with system size displacing the region of the MPS globule. It is quite likely that the thermodynamically stable MPS globule for heteropolymers of several hundreds of monomers is possible only for a narrow class of some special sequences. Also it is likely that inclusion of other interactions, such as electrostatic, and thus modification of the two-body interaction matrix in Eq. (2), may additionally stabilise the MPS globule.

We find that the kinetics of folding from the coil to the MPS globule for copolymers takes much longer than for the homopolymer since it is strongly affected by the presence of the transient frustrated states along the kinetic pathway. This leads to a complicated kinetic process consisting of multiple steps with pronounced slowing down and then acceleration in the folding rate. We also present here some preliminary studies on how the folding kinetics depends on the primary heteropolymer sequence. Typically, the kinetics for copolymers consisting of long blocks proceeds in a smaller number of steps, but not necessarily faster, than kinetics for short block copolymers. For the latter we have seen that even small modifications of the sequence may change crucially the overall kinetic behaviour and even the final kinetic state itself.

There is an interesting arena here for classification of sequences and conformational states. Moving in this direction would allow to develop better models for proteins, which sequences have been specially optimised by the biological evolution.

Finally, we hope that the way is now open for constructing the non-Gaussian extension to the self-consistent method. This is difficult since the closure relations for higher-order correlation functions are nontrivial for polymers. When that is accomplished one could speak of real predictive accuracy of the method.

\* \* \*

The authors acknowledge interesting discussions with Professor A.Yu. Grosberg, Professor K. Kawasaki, Professor G. Parisi, Dr D.A. Tikhonov, Dr R.V. Polozov and our colleagues Professor K.A. Dawson, Dr A.V. Gorelov and A. Moskalenko. The authors acknowledge the support of the Centre for High Performance Computing Applications, University College Dublin, Ireland.

#### REFERENCES

- [1] T. OHTA, and K. KAWASAKI, *Macromolecules*, **19** (1986) 2621; L. LEIBLER, *Macromolecules*, **13** (1980) 1602; G. H. FREDRICKSON, and E. HELFAND, *J. Chem. Phys.*, **87** (1987) 697; T. HASHIMOTO, *Macromolecules*, **20** (1987) 465; T. GAREL, and H. ORLAND, *Europhys. Lett.*, **6** (4) (1988) 307; **6** (1988) 597; G. H. FREDRICKSON, S. T. MILNER, and L. LEIBLER, *Macromolecules*, **25** (1992) 6341.
- [2] M. L. HUGGINS, *J. Chem. Phys.*, **9** (1941) 440; P. J. FLORY, *J. Chem. Phys.*, **9** (1941) 660; *Polymer Blends*, edited by D. R. PAUL, and S. NEUMAN, (Academic Press, 1987); *Multicomponent Polymer Systems*, edited by I. S. MILES, and S. ROSTAMI, (Longman Scientific and Technical, Singapore, 1992).
- [3] E.G. TIMOSHENKO, YU.A. KUZNETSOV, and K.A. DAWSON, *J. Chem. Phys.*, **102** (1995) 1816.
- [4] YU.A. KUZNETSOV, E.G. TIMOSHENKO, and K.A. DAWSON, *J. Chem. Phys.*, **104** (1996) 3338.
- [5] E.G. TIMOSHENKO, YU.A. KUZNETSOV, and K.A. DAWSON, *Phys. Rev.*, **E 53** (1996) 3886.
- [6] G. ALLEGRA, and F. GANAZZOLI, *J. Chem. Phys.*, **83** (1985) 397; G. RAOS, and G. ALLEGRA, *J. Chem. Phys.*, **104** (1996) 1626.
- [7] E.G. TIMOSHENKO, YU.A. KUZNETSOV, and K.A. DAWSON, submitted to *Phys. Rev. E*.
- [8] M. DOI, S. F. EDWARDS, *The Theory of Polymer Dynamics* (Oxford Science, NY, 1989).
- [9] P. G. DE GENNES, *Scaling Concepts in Polymer Physics* (Cornell Univ. Press, NY, 1988).
- [10] J. DES CLOIZEAUX, and G. JANNINK, *Polymers in Solution* (Clarendon Press, Oxford, 1990).
- [11] In what follows we fix the units of temperature, size and time by choosing  $k_B T = 1$ ,  $l = 1$  and  $\zeta_b = 1$ . We account for the volume interactions up to three-body terms, i.e. we assume that  $u_{\{n\}}^{(J)} = 0$  for  $J > 3$ . Taking into consideration of the self-interaction term (18), to prevent collapse of monomers for any negative second virial coefficient, is sufficient if the third virial coefficient is positive. below we also fix the third virial coefficient,  $u^{(3)} = 10$ .
- [12] A. YU. GROSBERG, A. R. KHOKHLOV, *Statistical Physics of Macromolecules* (AIP, NY, 1994).
- [13] YU.A. KUZNETSOV, E.G. TIMOSHENKO, and K.A. DAWSON, *J. Chem. Phys.*, **102** (1995) 4807.

- [14] The total collapse time,  $\tau_t$ , defined as that time, when the squared radius of gyration has passed through 99% of its overall change:  $R_g^2(\tau_t) = 0.01 R_g^2(0) + 0.99 R_g^2(\infty)$ . The final relaxation,  $\tau_f$ , determined from the mean squared radius of gyration  $R_g^2(t) = R_g^2(\infty) + A_f e^{-t/\tau_f}$ , or equivalently the time-scale deduced from the first internal mode  $\mathcal{F}_1(t)$  (see Ref. [4] for more details).
- [15] YU.A. KUZNETSOV, E.G. TIMOSHENKO, *J. Chem. Phys.*, **111** (1999) 3744.
- [16] W. H. PRESS, S. A. TEUKOLSKY, W. T. VETTERLING, and B. P. FLANNERY, *Numerical Recipes in C* (Cambridge University Press, 1992).
- [17] M. MEZARD, G. PARISI, and M. VIRASORO, *Spin glass theory and beyond* (World Scientific, Singapore, 1987).

TABLE I. – Values of the mean squared radius of gyration,  $R_g^2$ , for the globular state at equilibrium,  $u^{(2)} = -25$  and  $u^{(3)} = 10$ , and characteristic collapse times,  $\tau_t$  and  $\tau_f$  after the quench  $u^{(2)} = 15 \rightarrow -25$  for different lengths of polymer ring,  $N$ . Data for  $c_3 = 3$  and  $c_3 = 0$  correspond to the prescription with and without self-interaction term (18). The last column contains the effective exponent of the appropriate quantity in terms of the degree of polymerization, i.e.  $A \sim N^\gamma$ .

$N$	30	50	70	100	150	200	300	exponent
$R_g^2(c_3 = 0)$	1.19	1.91	2.59	3.53	4.96	6.25	8.52	$2\nu = 0.86 \pm 0.03$
$R_g^2(c_3 = 3)$	0.91	1.32	1.68	2.17	2.90	3.55	4.72	$2\nu = 0.69 \pm 0.01$
$\tau_t(c_3 = 0)$	3.9	10.5	20.3	40.8	90.7	160.3	357	$\gamma_t = 1.96 \pm 0.01$
$\tau_t(c_3 = 3)$	3.4	8.4	14.8	27.3	53.3	89.1	179	$\gamma_t = 1.70 \pm 0.03$
$\tau_f(c_3 = 0)$	1.18	2.97	5.49	10.2	20.6	33.0	65.7	$\gamma_f = 1.74 \pm 0.03$
$\tau_f(c_3 = 3)$	0.73	1.41	2.66	4.25	7.34	9.92	16.8	$\gamma_f = 1.27 \pm 0.05$

Fig. 1. – Diagram of stability of the liquid-like versus the non-compact globules in term of the second virial coefficient,  $u^{(2)}$ , and the self-interaction parameter,  $c_3$ . Curve I corresponds to discontinuous transition, curves I' and I'' are spinodals.

Fig. 2. – Plot of the mean squared distances between monomers,  $D_{0m}$ , versus the chain index,  $m$ , for polymer with  $N = 200$  for the non-compact (NCG),  $c_3 = 0$ , and the liquid-like (LLG) globules,  $c_3 = 3$ . Here  $u^{(2)} = -25$  and  $u^{(3)} = 10$ . In the right-hand side we present the data from Monte Carlo simulations [?] for the same polymer size. Since the function  $D_{0m}$  is symmetric with respect to the value  $N/2$  we present these dependencies only on half-interval.

Fig. 3. – Plot of the mean squared radius of gyration,  $R_g^2$  versus time,  $t$ , at the kinetics of the collapse transition,  $u^{(2)} = 15 \rightarrow -25$  to the non-compact (NCG),  $c_3 = 0$ , and the liquid-like (LLG),  $c_3 = 3$ , globules.

Fig. 4. – The phase diagram of “random” sequence ‘ $babca_2cbac_2acb_3cac_3a_2b_2cac_2b'$ ’ in terms of the mean second virial coefficient,  $\bar{u}^{(2)}$ , and the amphiphilicity,  $\Delta$ . Curves (Collapse) and (MPS) correspond respectively to the collapse and the micro-phase separation continuous transitions. Curves (I) and (II) correspond to discontinuous transitions to the frustrated phases. “Spinodal” curves (I') and (II') bound the regions of metastability of the frustrated states. Transition curves and boundaries distinguishing different frustrated states are not depicted.

Fig. 5. – The phase diagram of “random” sequence ‘ $(babca_2cbac_2acb_3cac_3a_2b_2cac_2b)_2'$ ’, i.e. twice as in Fig. 4 in terms of the mean second virial coefficient,  $\bar{u}^{(2)}$ , and the amphiphilicity,  $\Delta$ . See caption to Fig. 4 for more details.

Fig. 6. – The phase diagram of “long block” copolymer sequence ‘ $(b_3a_3)_5'$ ’ in terms of the mean second virial coefficient,  $\bar{u}^{(2)}$ , and the amphiphilicity,  $\Delta$ . Since the frustrated phases here are not accessible, the collapse for large amphiphilicity proceeds through the discontinuous transition (curve (I)) and it is accompanied by micro-phase separation. Curves (I') and (I'') are spinodals.

Fig. 7. – Plot of the mean squared radius of gyration,  $R_g^2$ , versus the mean second virial coefficient,  $\bar{u}^{(2)}$ , for '(ab)<sub>30</sub>' copolymer. Here and in Fig. 8  $\Delta = 30$ , solid lines correspond to values of observables in the main free energy minimum and dashed lines — in metastable minima.

Fig. 8. – Plot of the parameter of micro-phase separation,  $\Psi$ , versus the mean second virial coefficient,  $\bar{u}^{(2)}$ , for '(ab)<sub>30</sub>' copolymer. See also caption to Fig. 7 for more details.

Fig. 9. – Diagrams of the mean squared distances matrix,  $D_{mm'}$  for '(ab)<sub>30</sub>' copolymer and amphiphilicity,  $\Delta = 20$ . Diagrams (a-e) correspond respectively to the values of the mean second virial coefficient,  $u^{(2)} = 15, -11, -21, -30$  and  $-40$ . Diagram (f) corresponds to the homopolymer globule, for which  $u^{(2)} = -25$  and  $\Delta = 0$ . Indices  $m, m'$  start counting from the upper left corner. Each matrix element,  $D_{mm'}$  is denoted by a quadratic cell with varying degree of black colour, the darkest and the lightest cells corresponding respectively to the smallest and to the largest mean squared distances. The diagonal elements are not painted since by definition,  $D_{mm} = 0$ .

Fig. 10. – Plot of the mean squared radius of gyration,  $R_g^2$  (Fig. (a)), the MPS order parameter,  $\Psi$  (Fig. (b)) and the instantaneous free energy,  $\mathcal{A}$  (Fig. (c)) versus time,  $t$ , during kinetics after the quench from  $\bar{u}^{(2)} = 15, \Delta = 0$  to  $\bar{u}^{(2)} = -35, \Delta = 30$  for copolymer sequences with  $N = 50$ . Lines A-D in the figures correspond respectively to the following sequences: ' $c_{50}$ ' (homopolymer), ' $(ba)_{25}$ ', ' $a_2b_3a_3b_2a_3b_2a_2b_3(ba)_{15}$ ' and ' $(ba)_3b_2(ba)_9a_2(ba)_5b_2a_2(ba)_4$ '.

Fig. 11. – Plot of the mean squared radius of gyration,  $R_g^2$  (Fig. (a)), the MPS order parameter,  $\Psi$  (Fig. (b)) and the instantaneous free energy,  $\mathcal{A}$  (Fig. (c)) versus time,  $t$ , during kinetics after the same quench as in Fig. 10 for copolymer sequences with  $N = 50$ . Lines A, E, F in the figures correspond respectively to the following sequences: ' $c_{50}$ ' (homopolymer), ' $(b_5a_5)_5$ ' and ' $b_6a_4b_5a_5b_4a_6b_3a_7b_7a_3$ '.

Fig. 12. – Diagrams of the mean squared distances matrix,  $D_{mm'}(t)$  for '(ba)<sub>25</sub>' copolymer in kinetics after the same quench as in Fig. 10. Diagrams (a-d) correspond respectively to the following moments in time:  $t = 3.5, 5.75, 8.60$  and  $13.0$ . See also caption to Fig. 9 for more details.

Fig. 13. – The diagram of the mean squared distances matrix,  $D_{mm'}(t)$  for copolymer sequence ' $(ba)_3b_2(ba)_9a_2(ba)_5b_2a_2(ba)_4$ ' at the time moment  $t = 45$ , so that this conformation is close to the final equilibrium. Parameters of the quench are the same as in Fig. 10. See also caption to Fig. 9, 12 for more details.



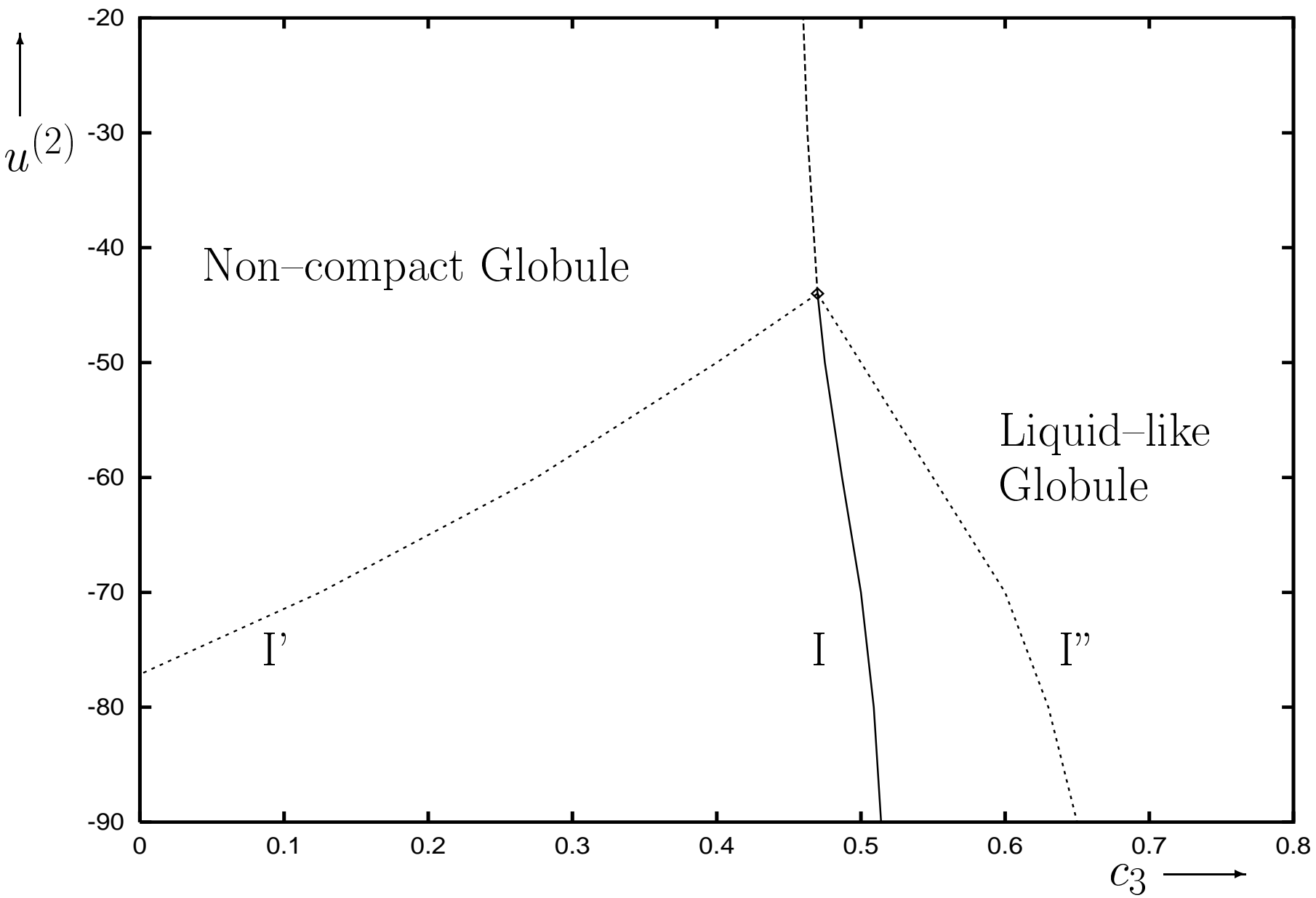


Fig. 1

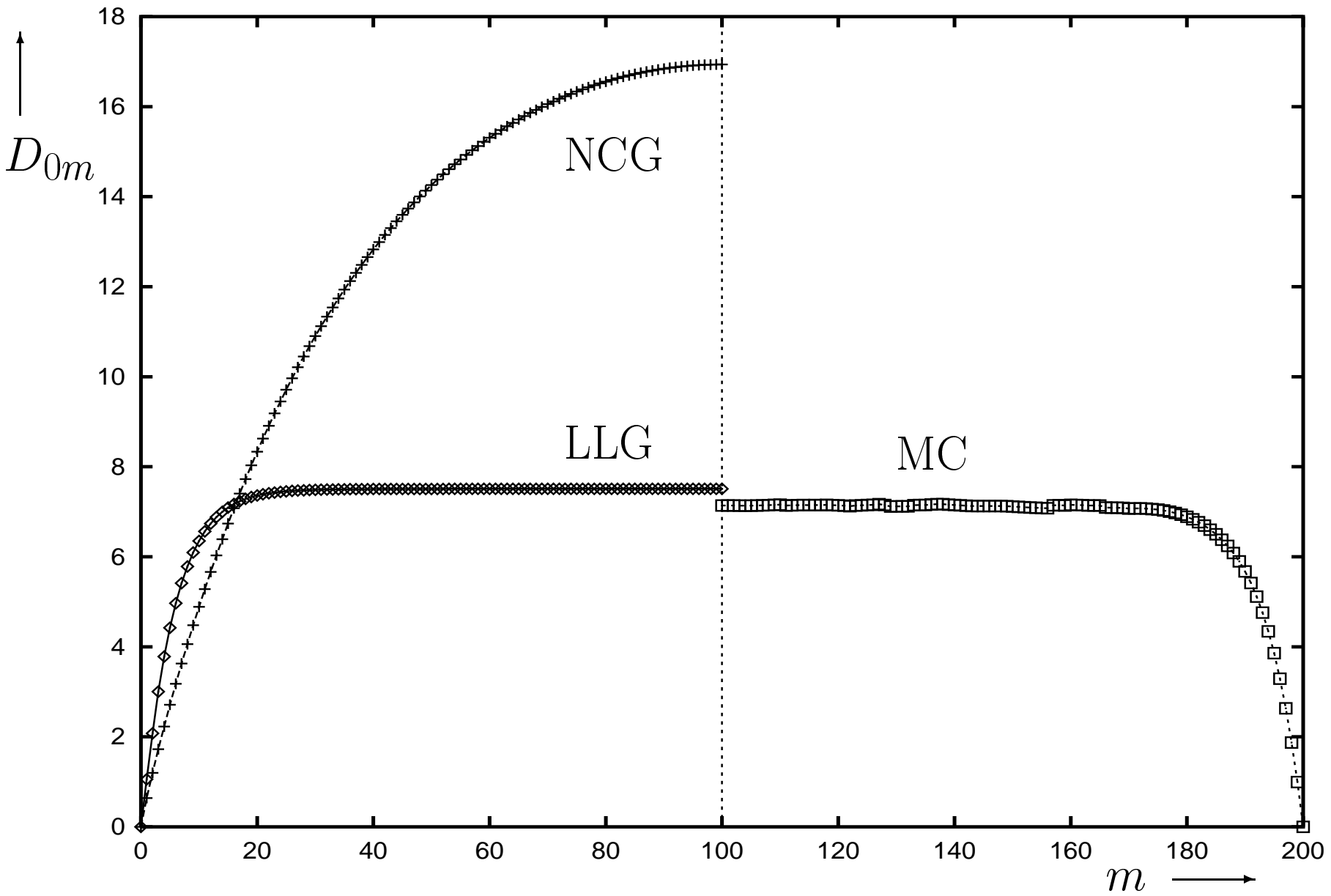


Fig. 2

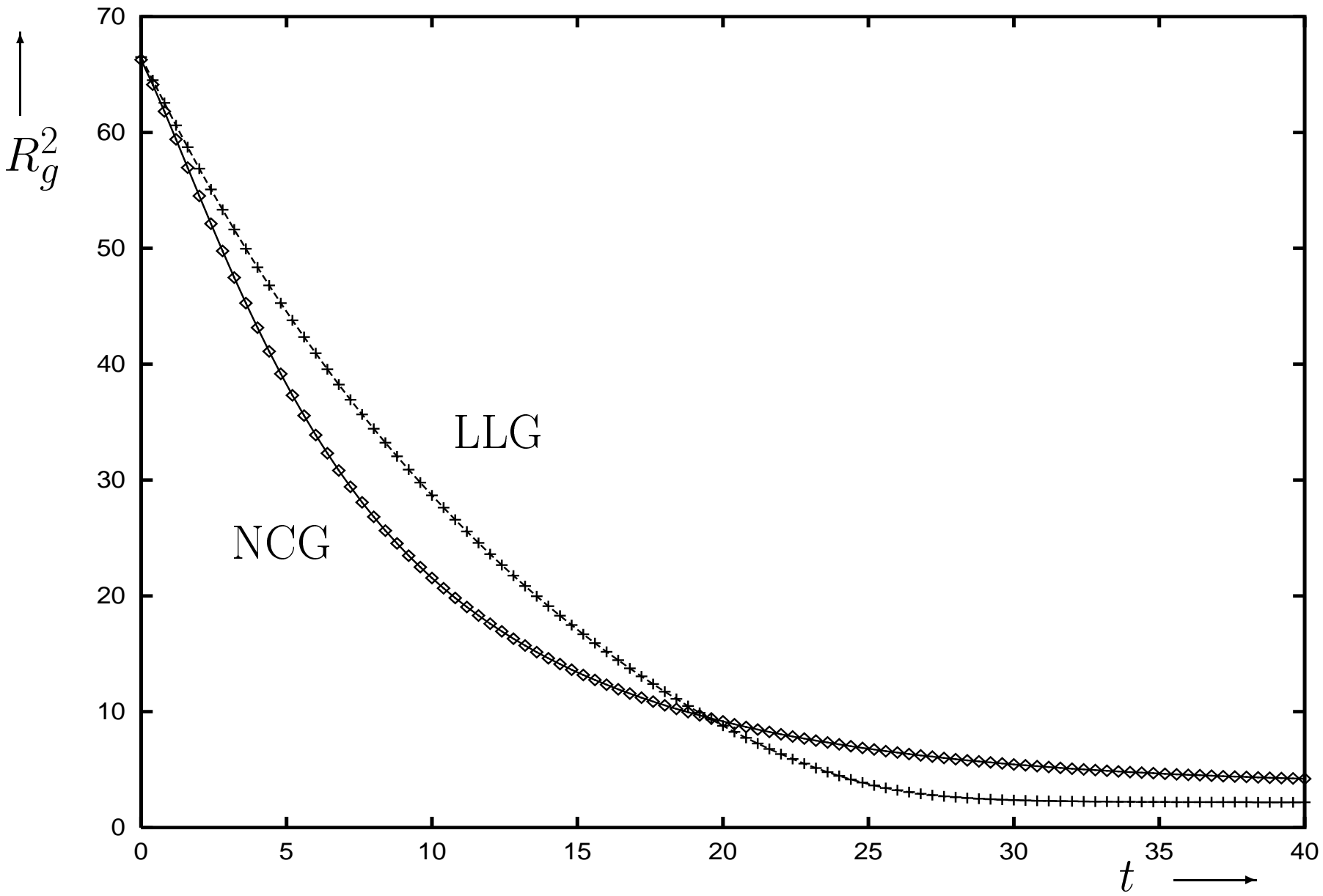


Fig. 3

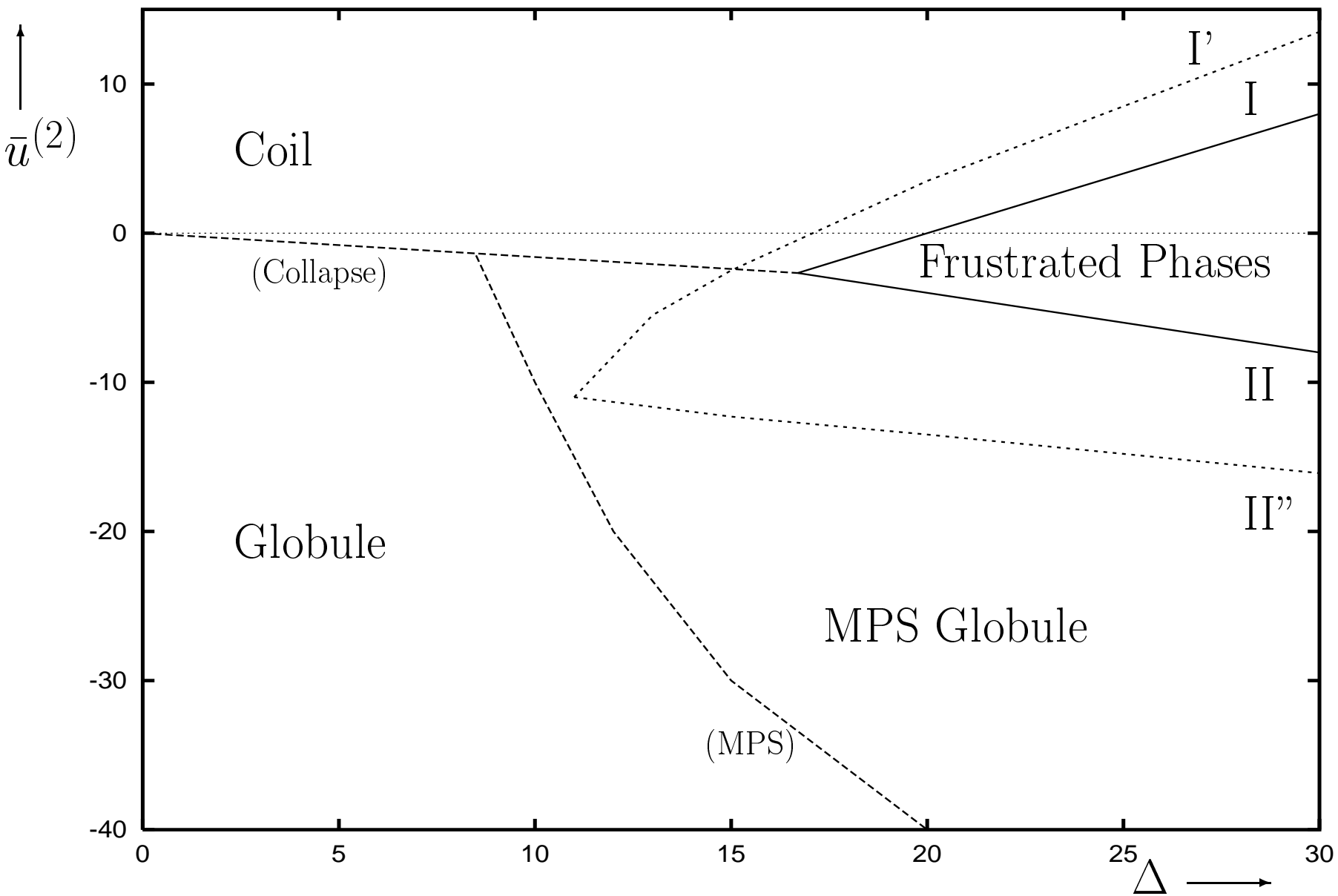


Fig. 4

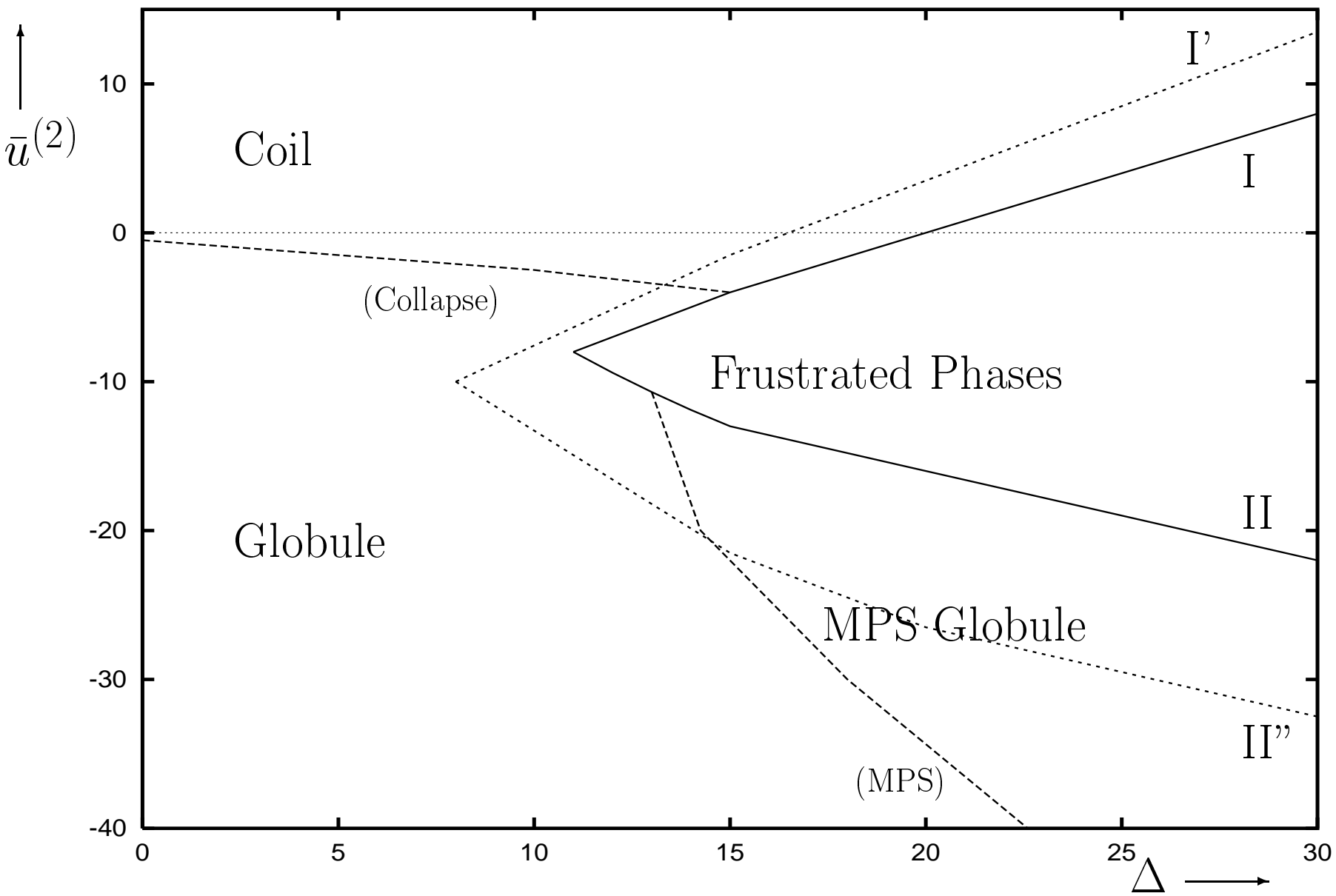
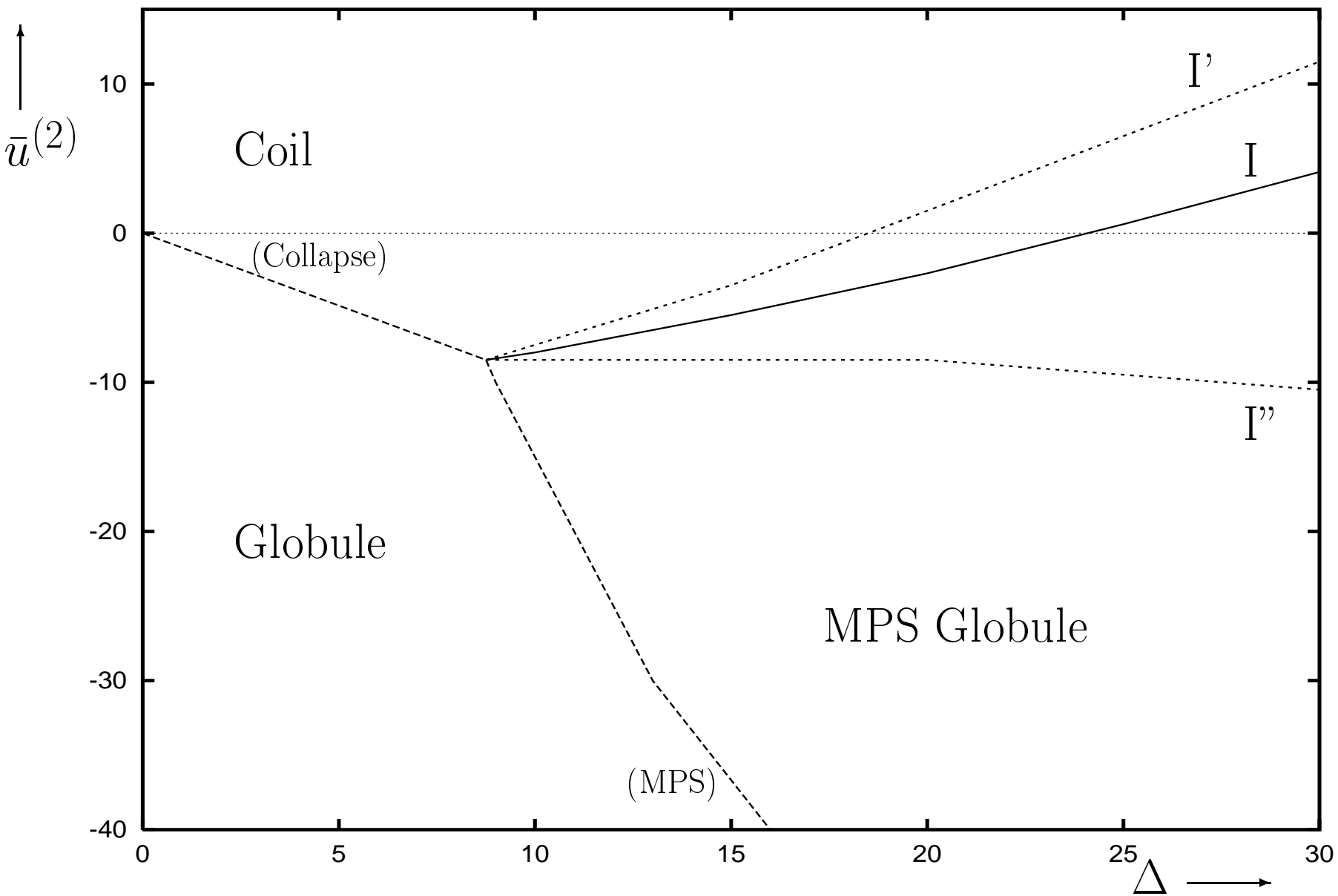


Fig. 5



**Fig. 6**

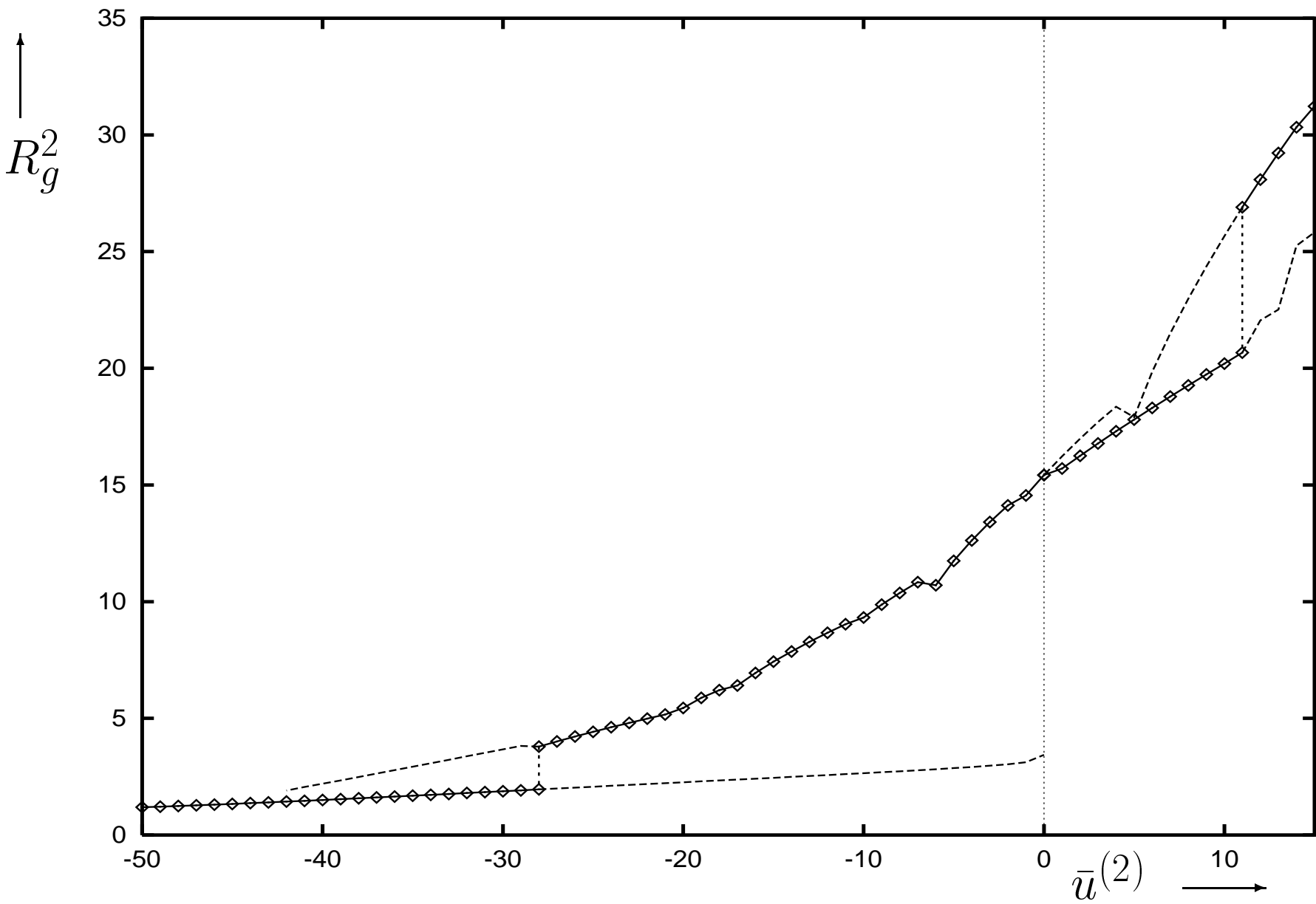


Fig. 7

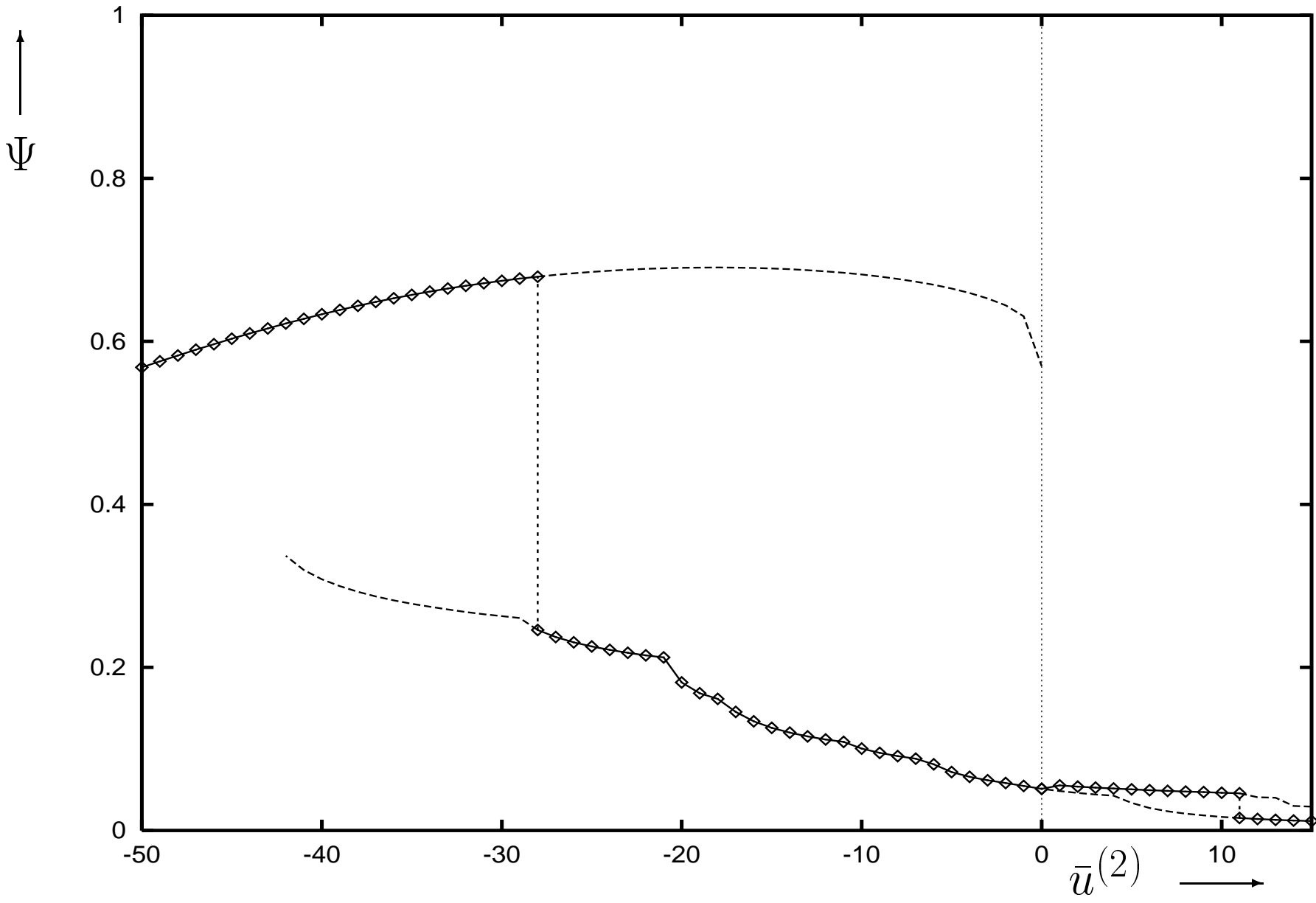


Fig. 8



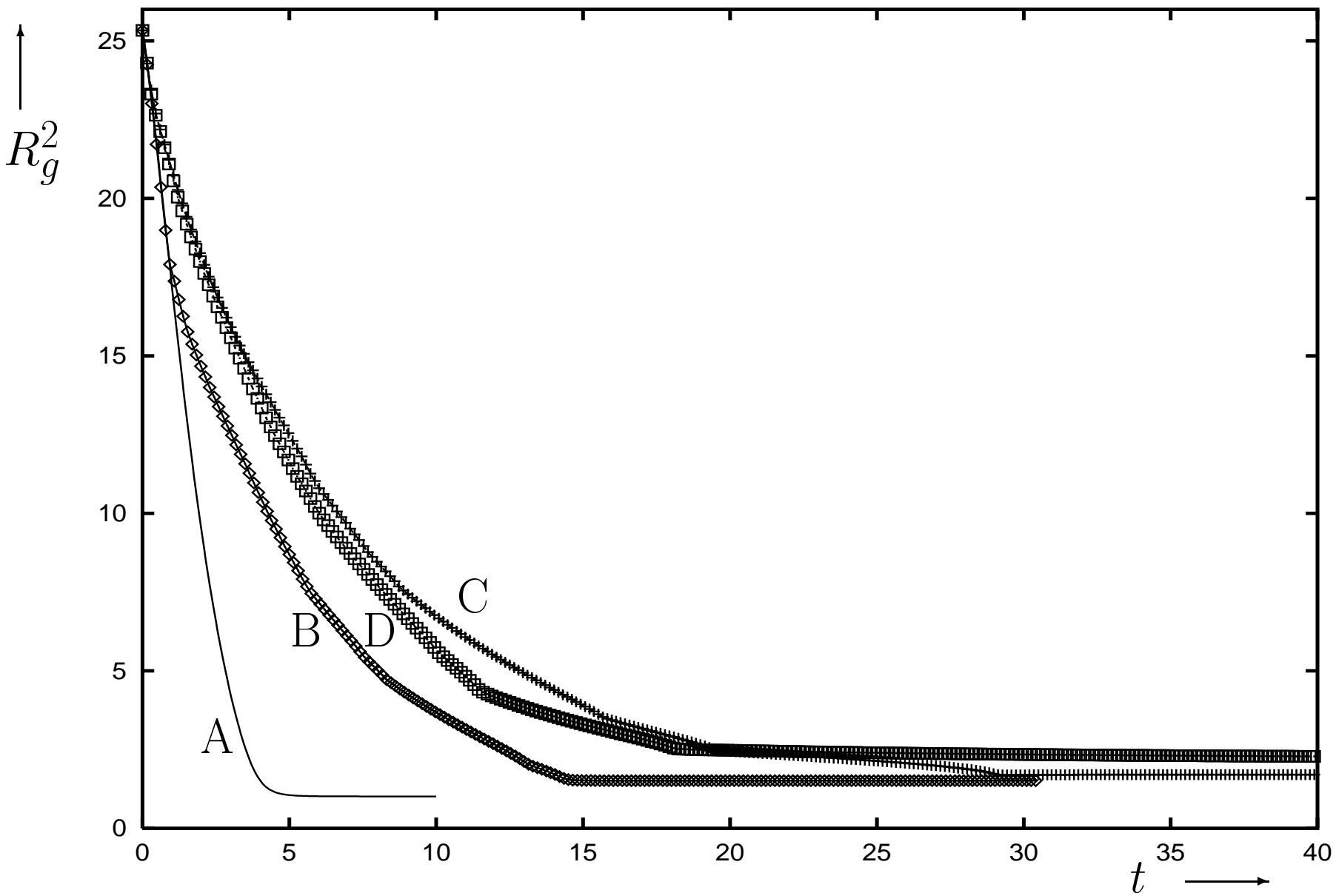


Fig. 10a

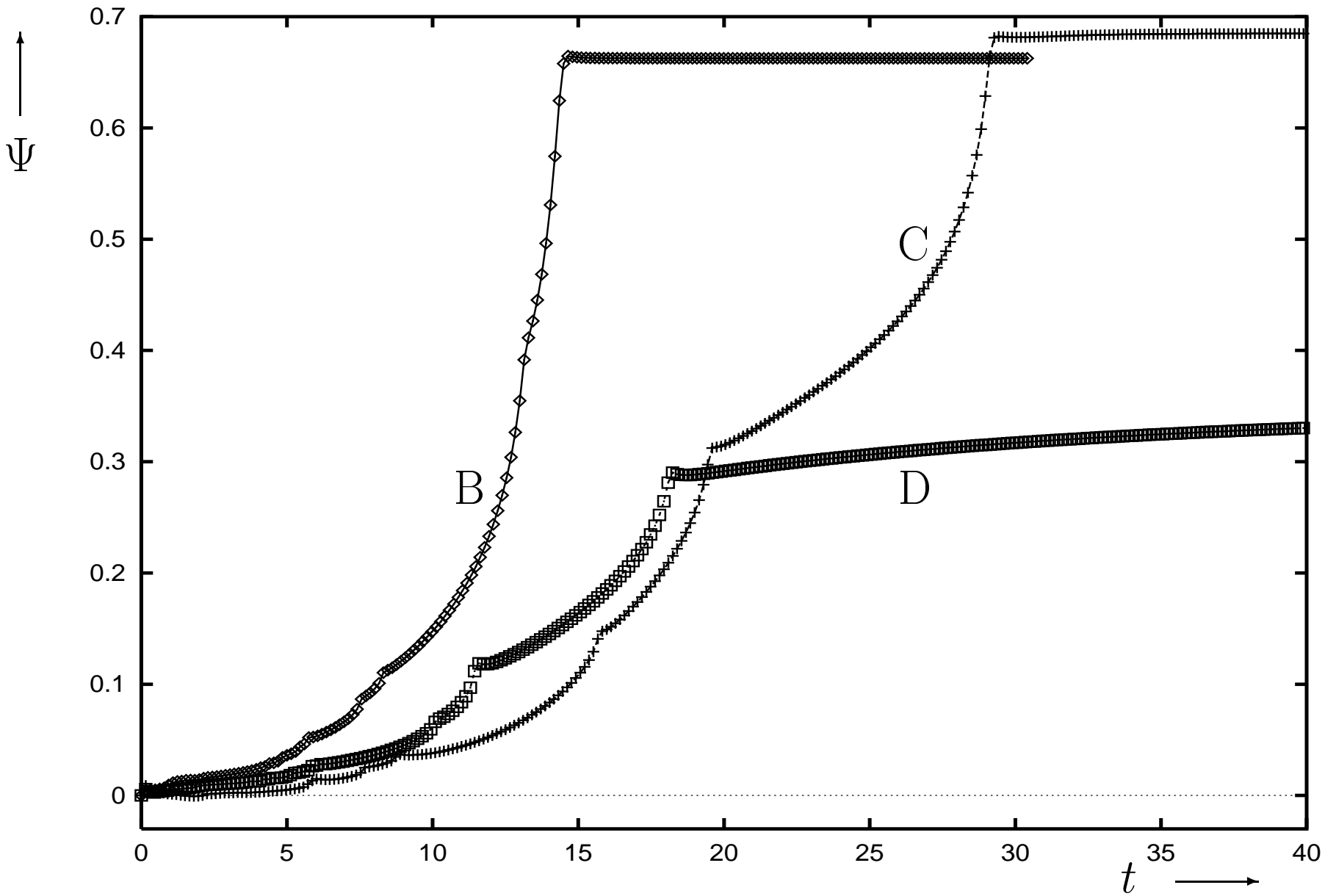


Fig. 10b

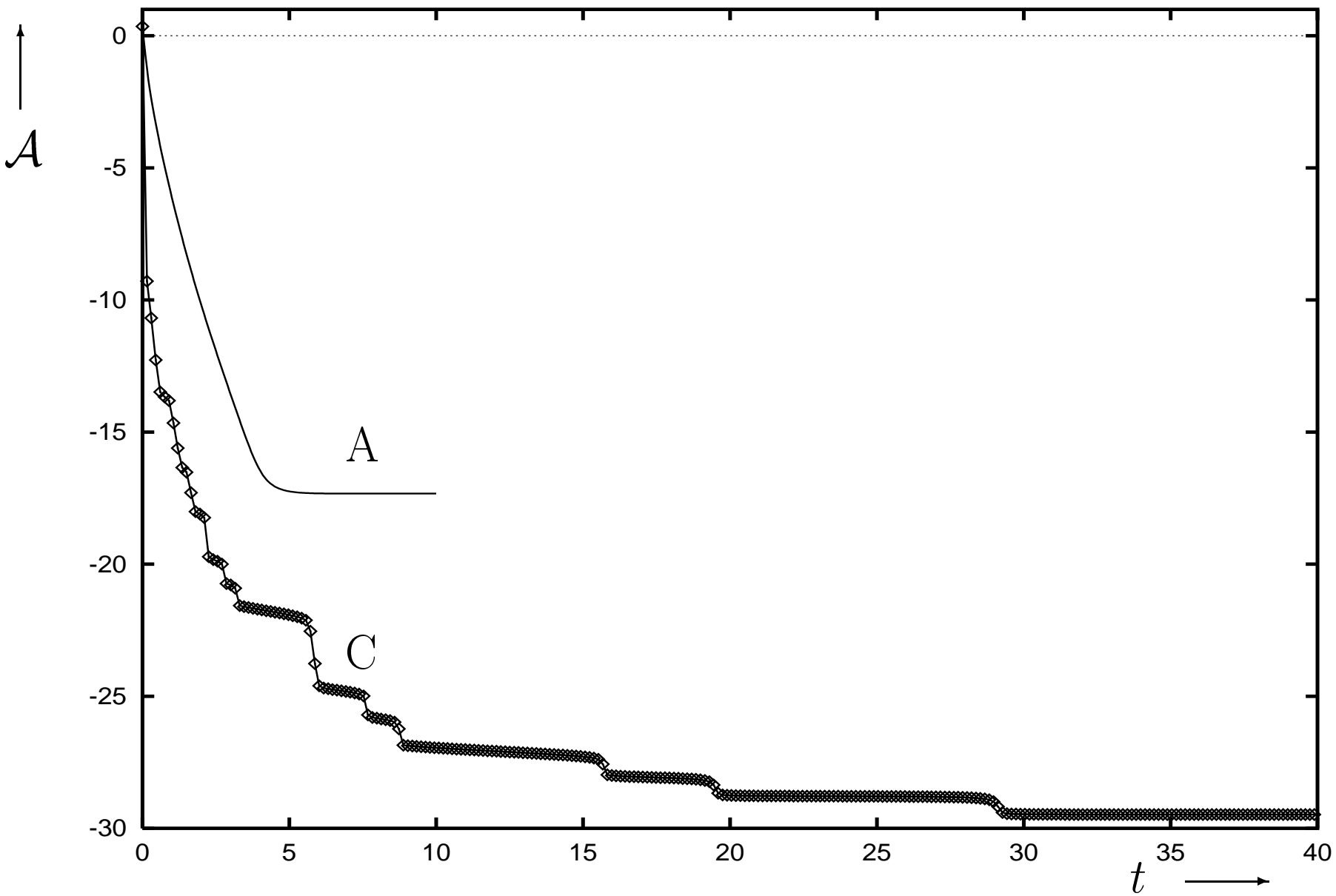


Fig. 10c

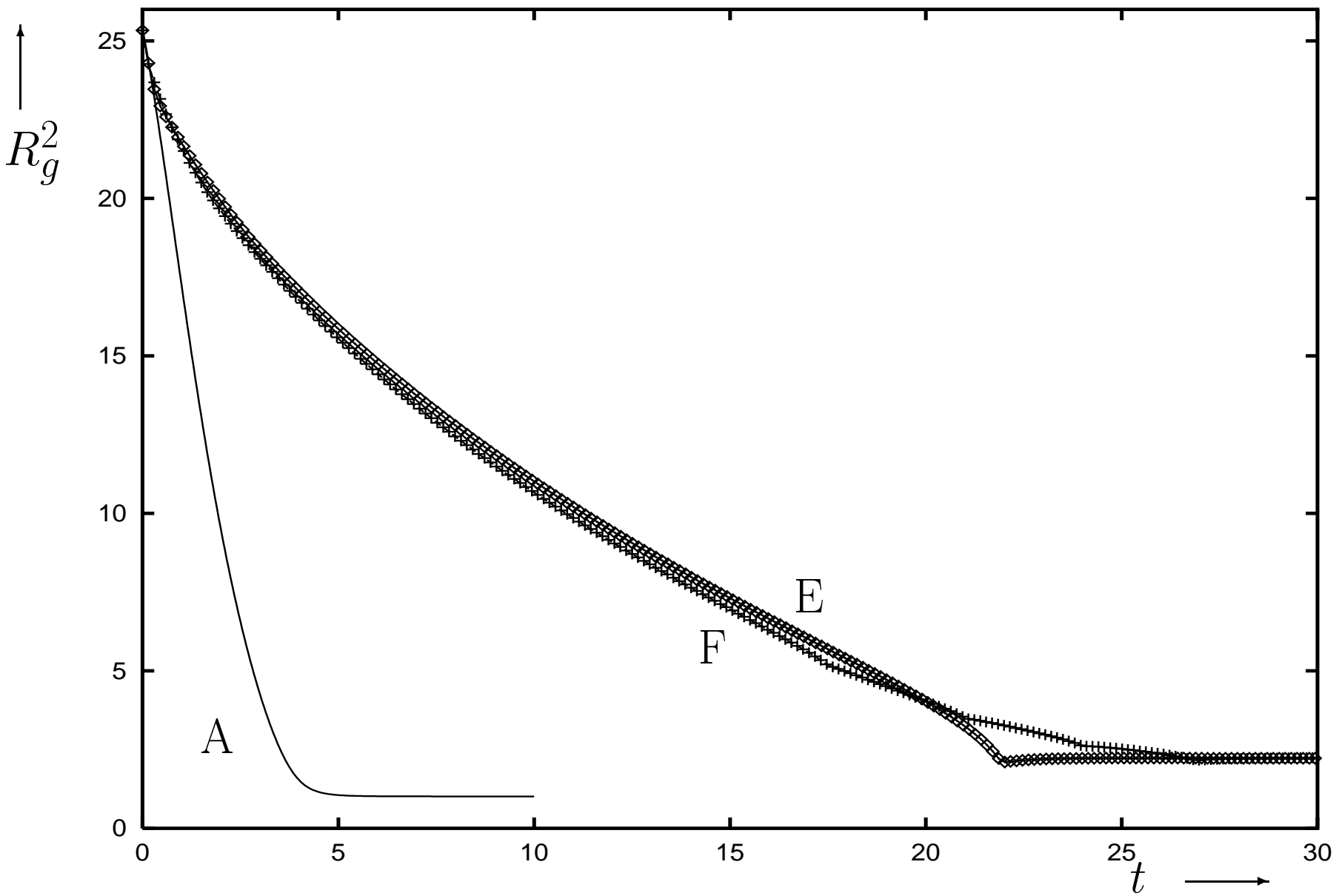


Fig. 11a

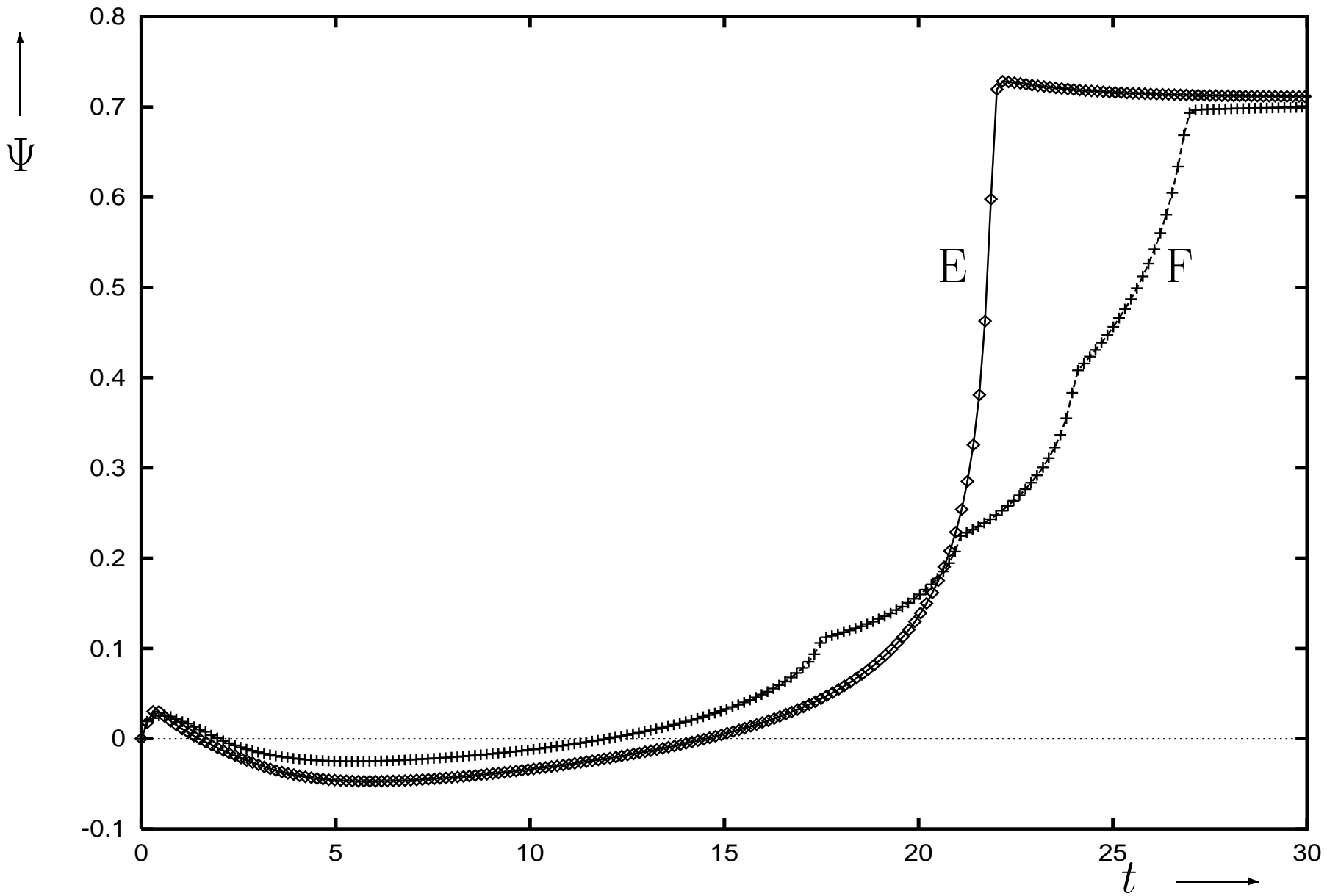


Fig. 11b

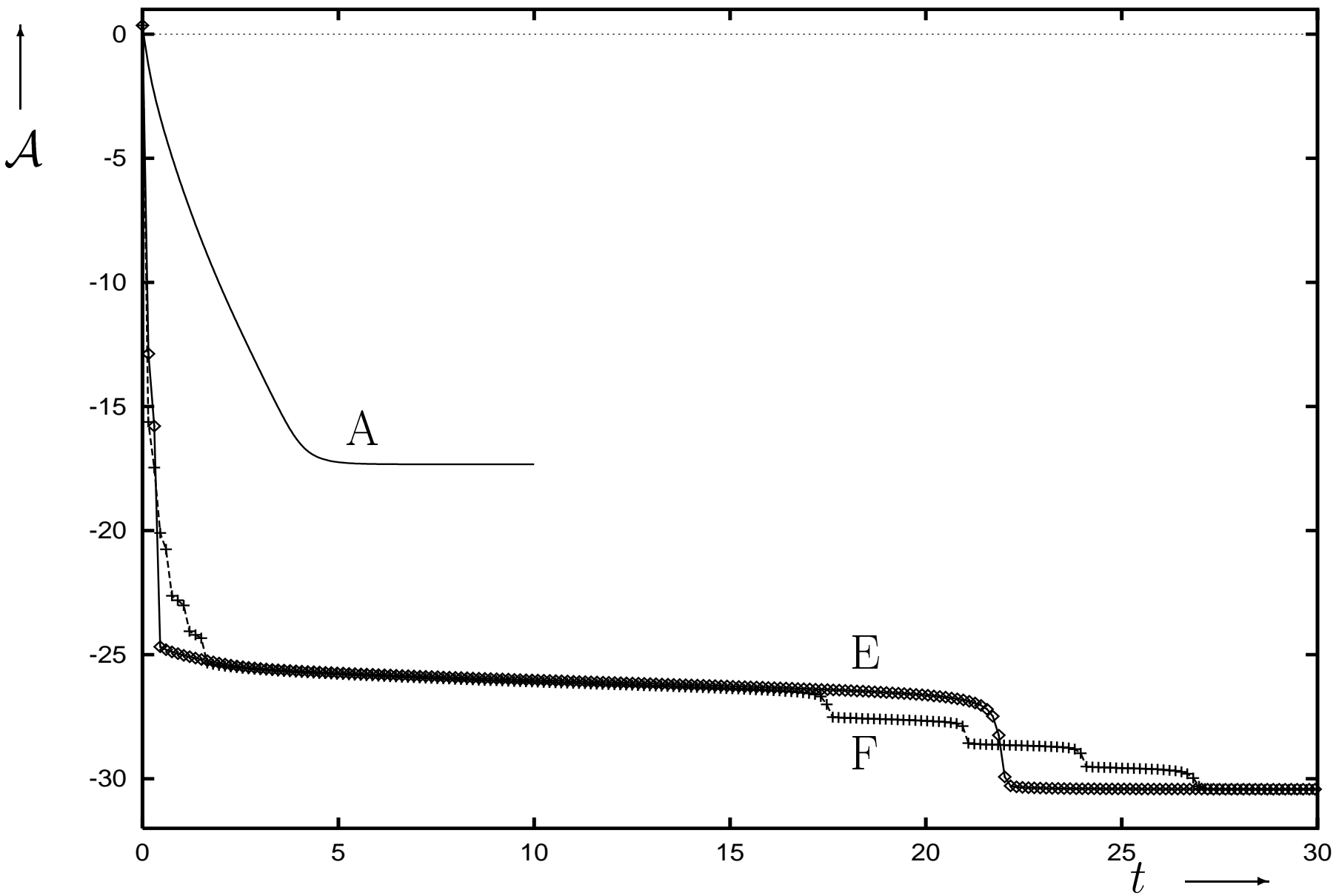


Fig. 11c

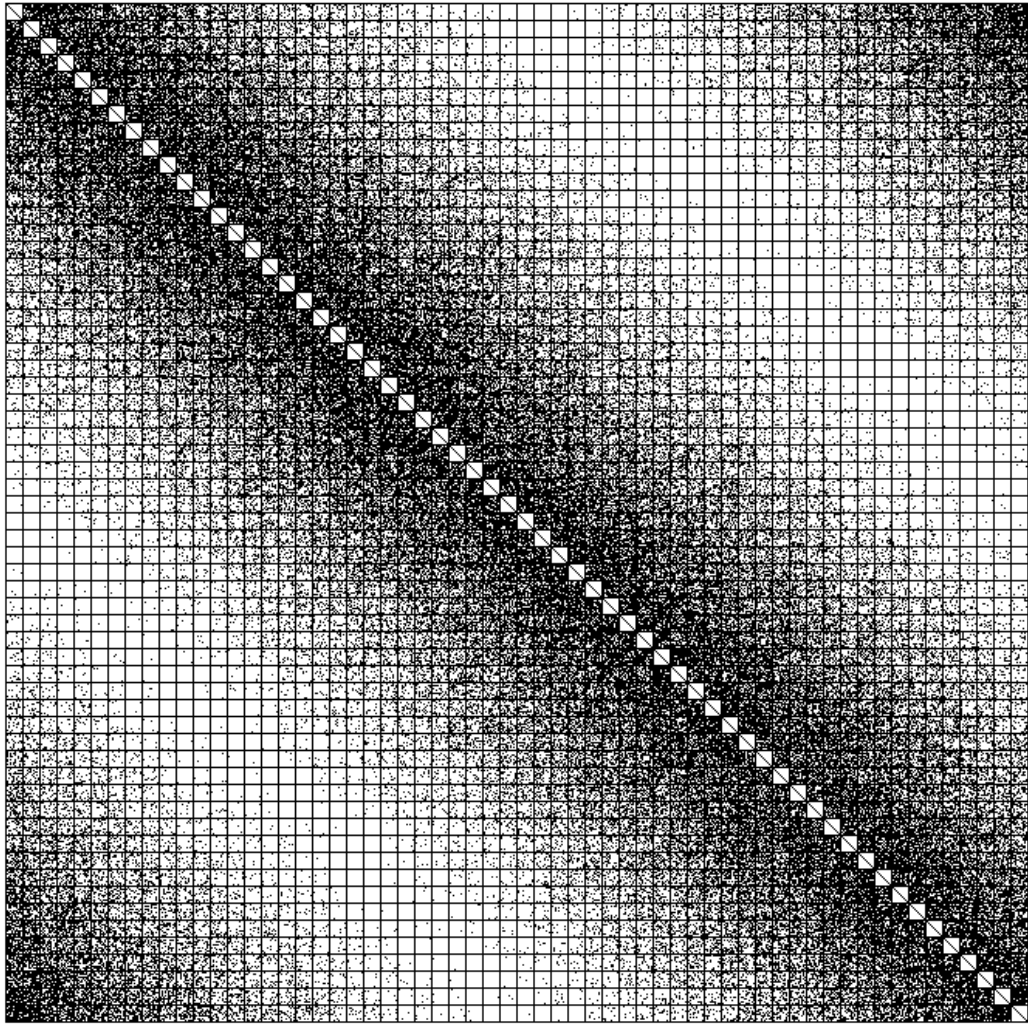


Fig. 9a

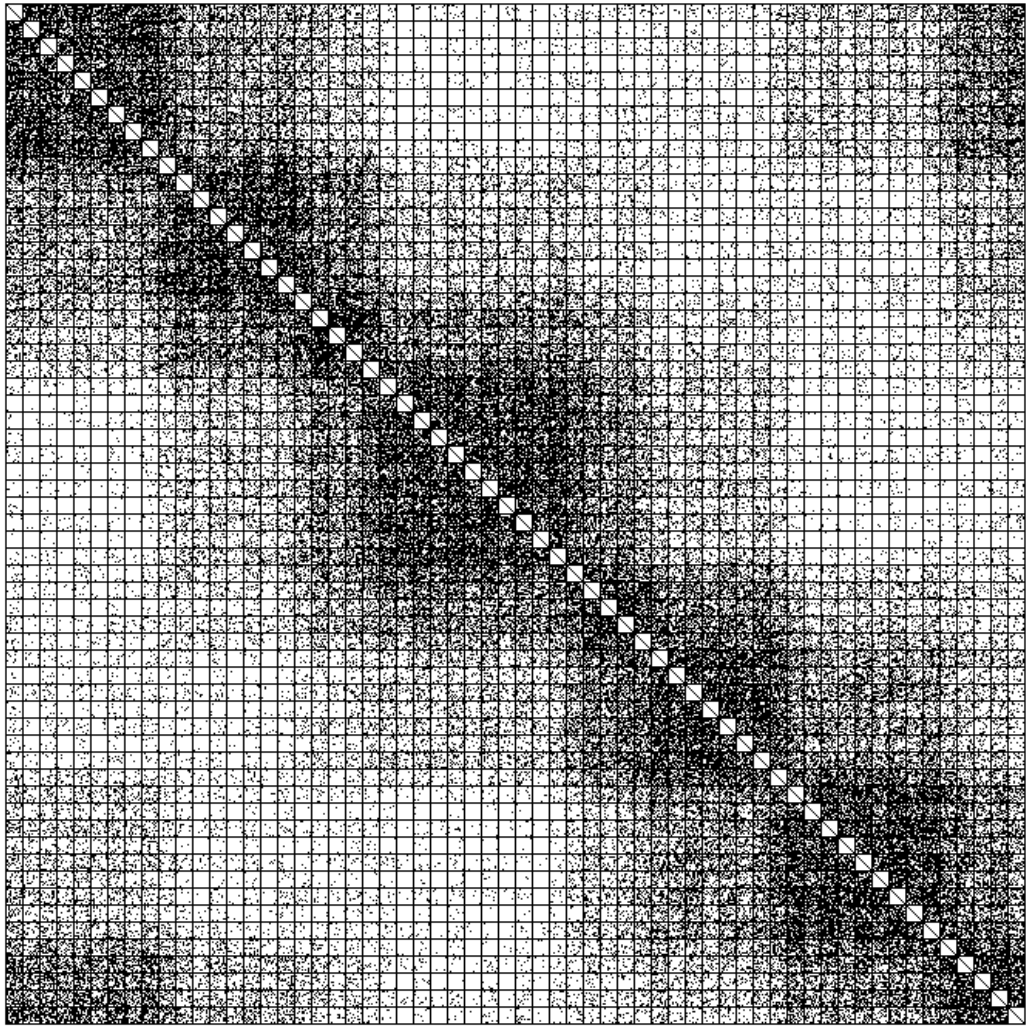


Fig. 9b



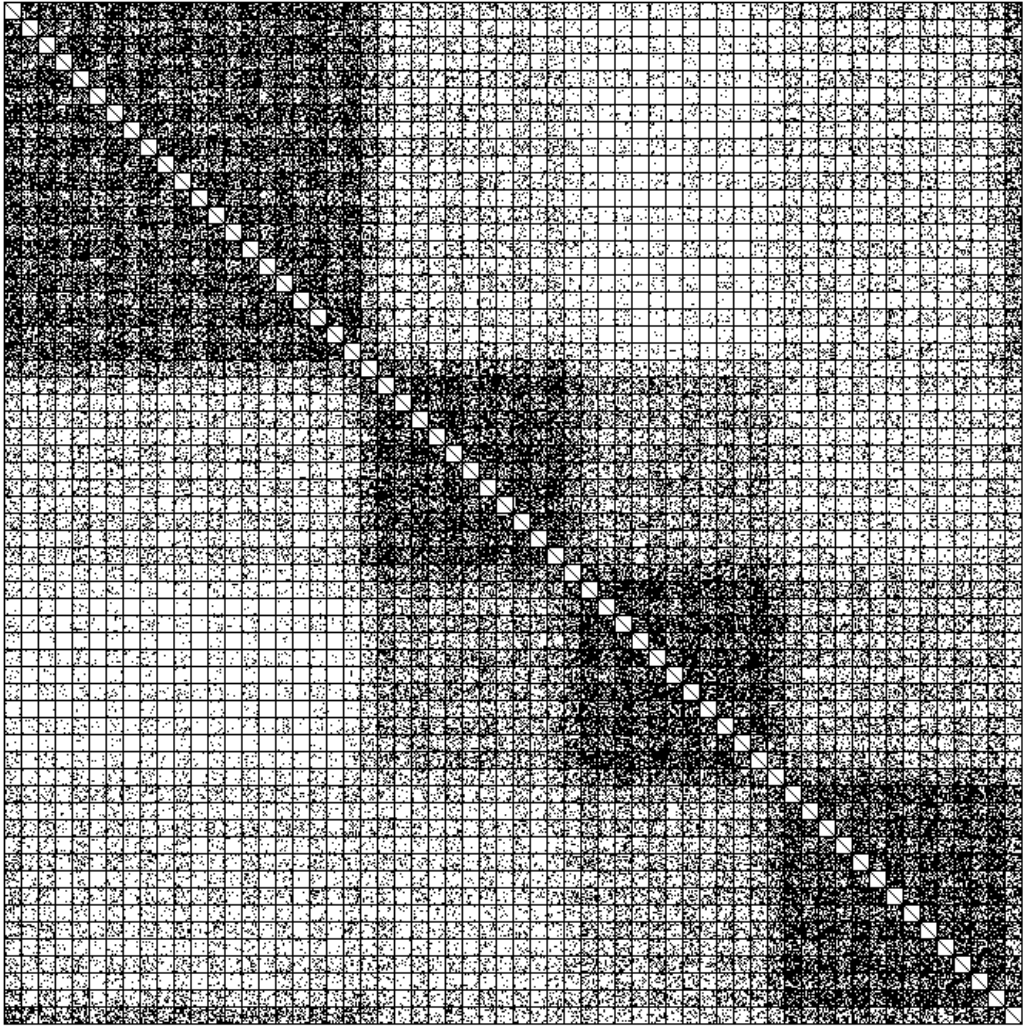


Fig. 9c

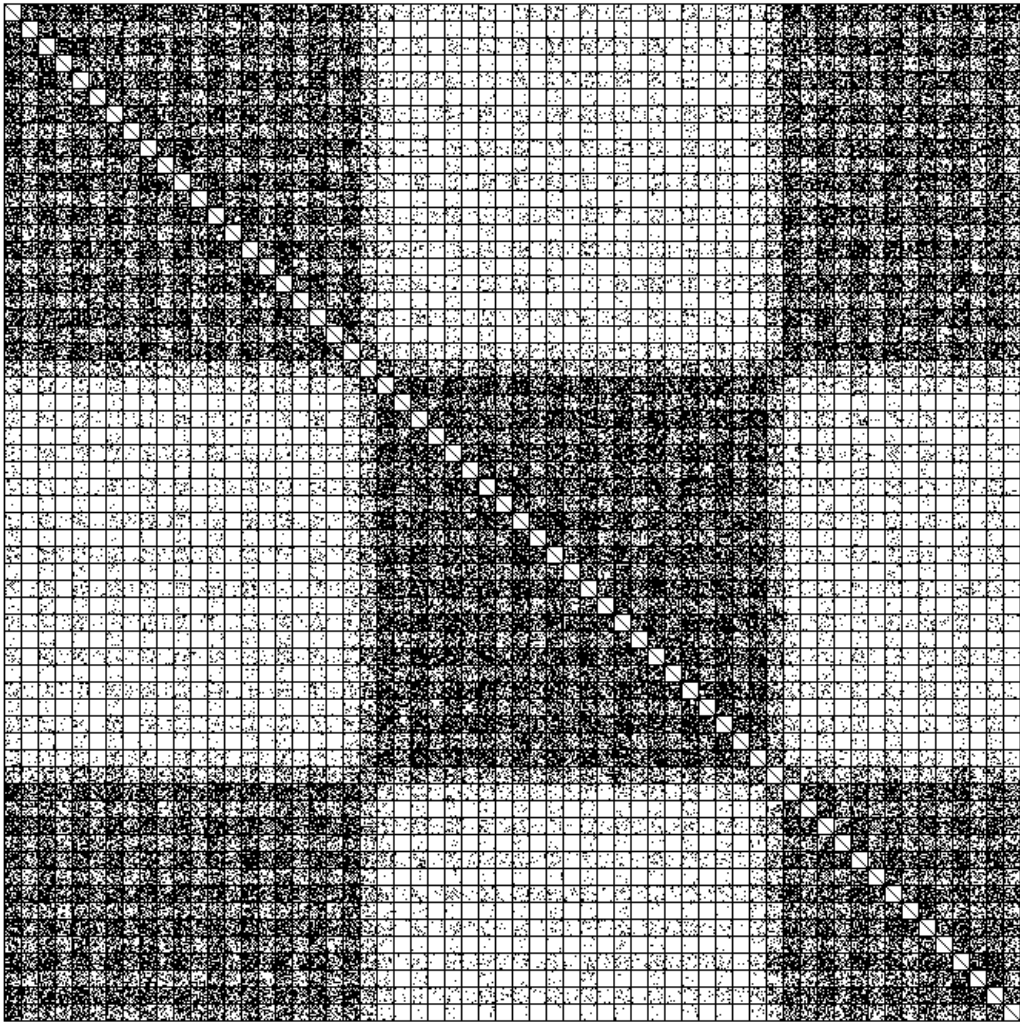


Fig. 9d

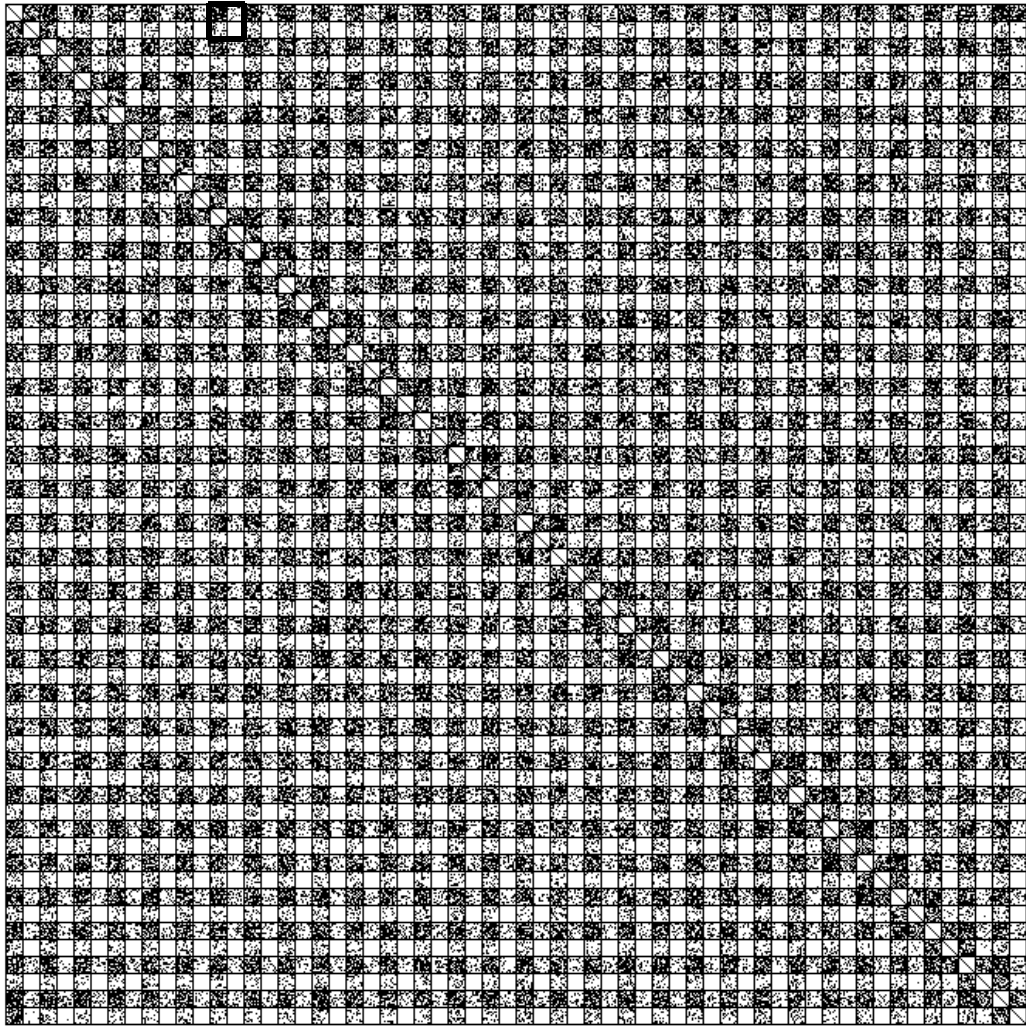


Fig. 9e

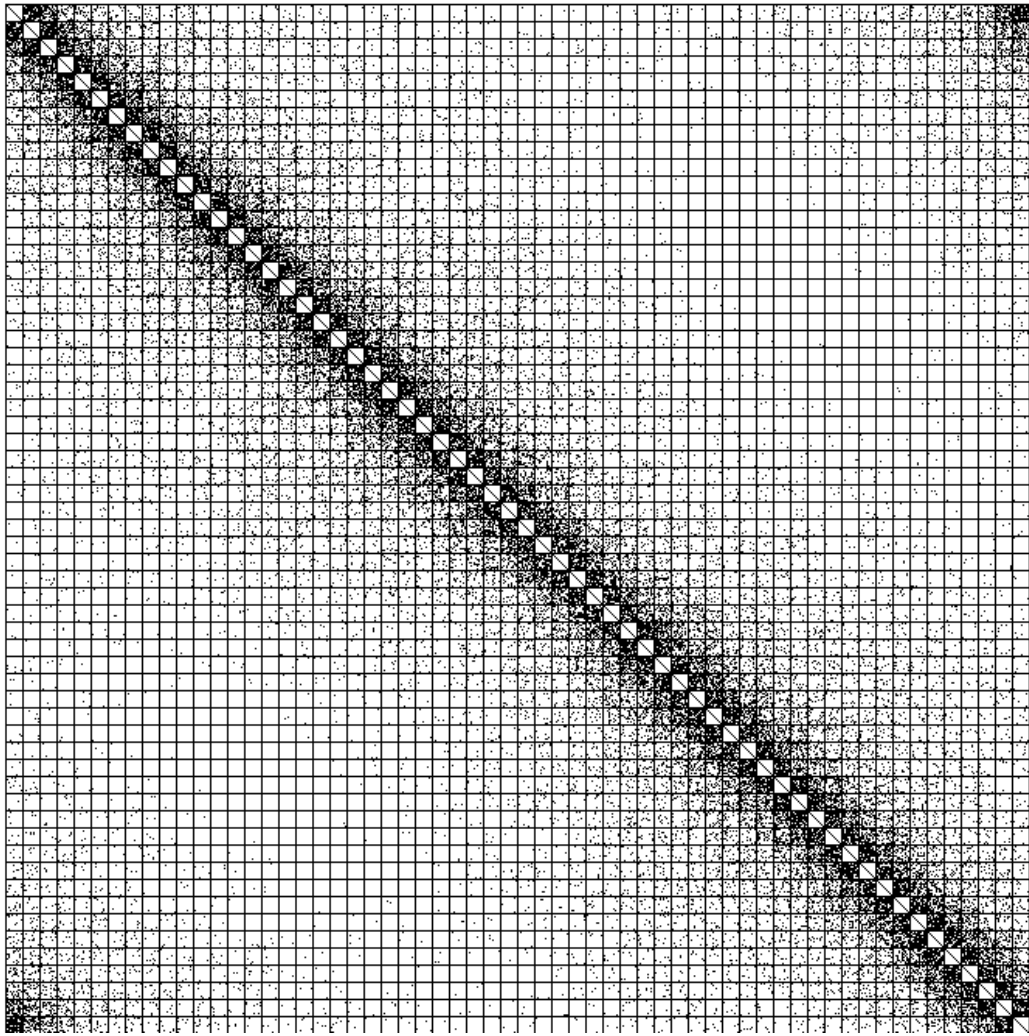


Fig. 9f

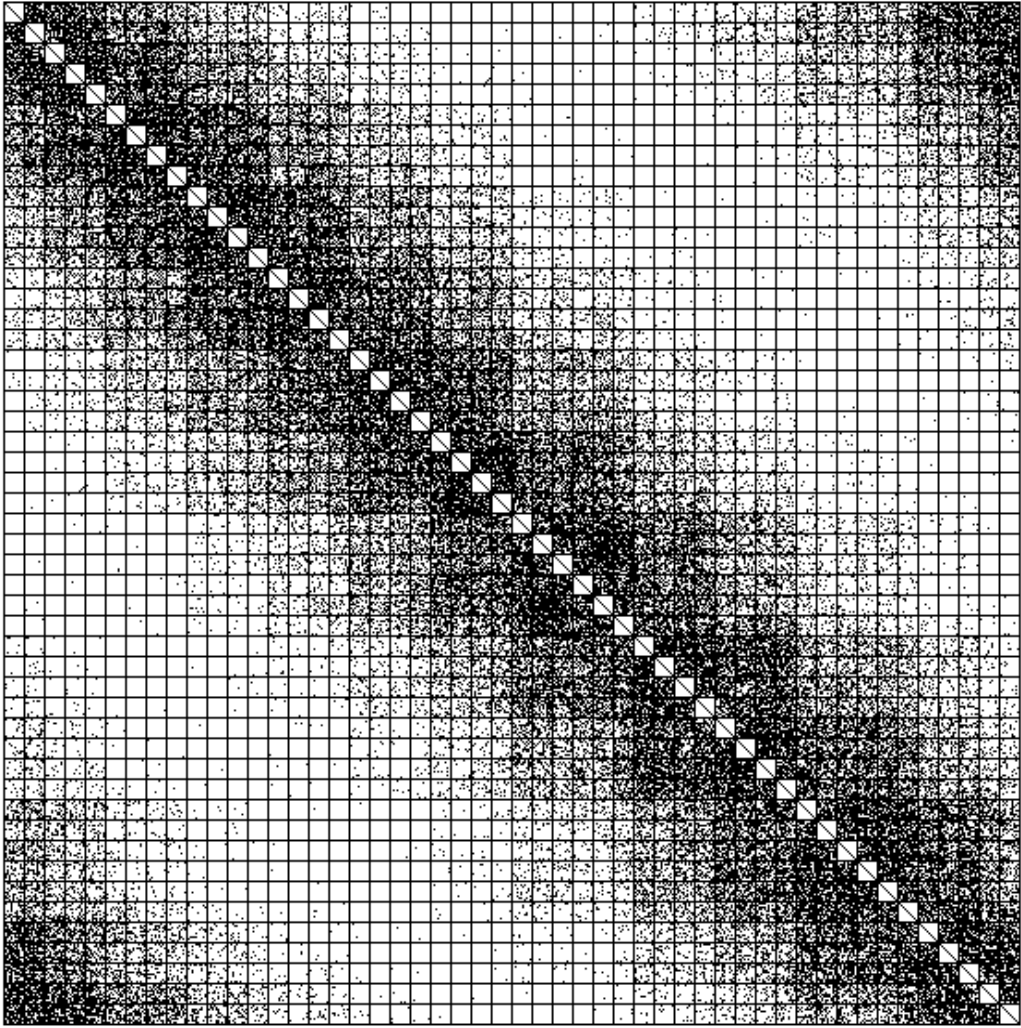


Fig. 12a

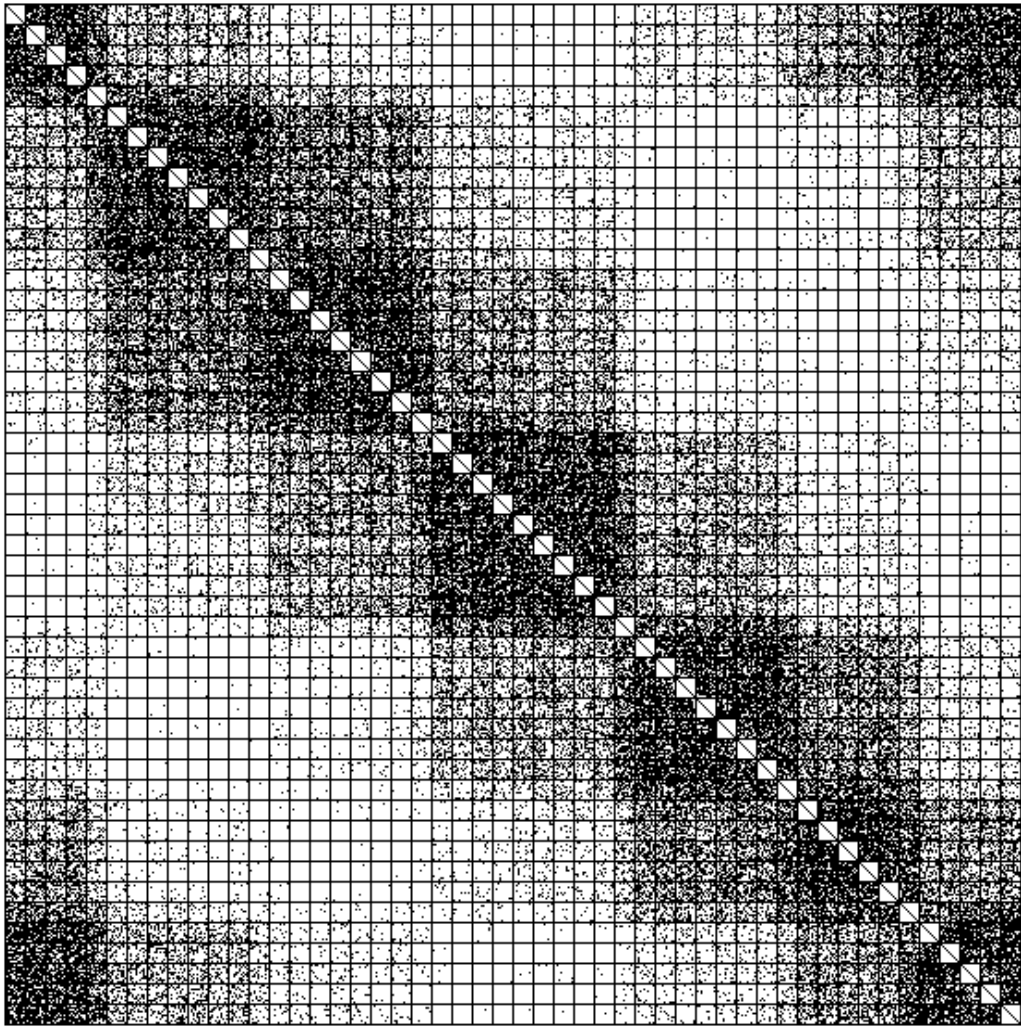


Fig. 12b

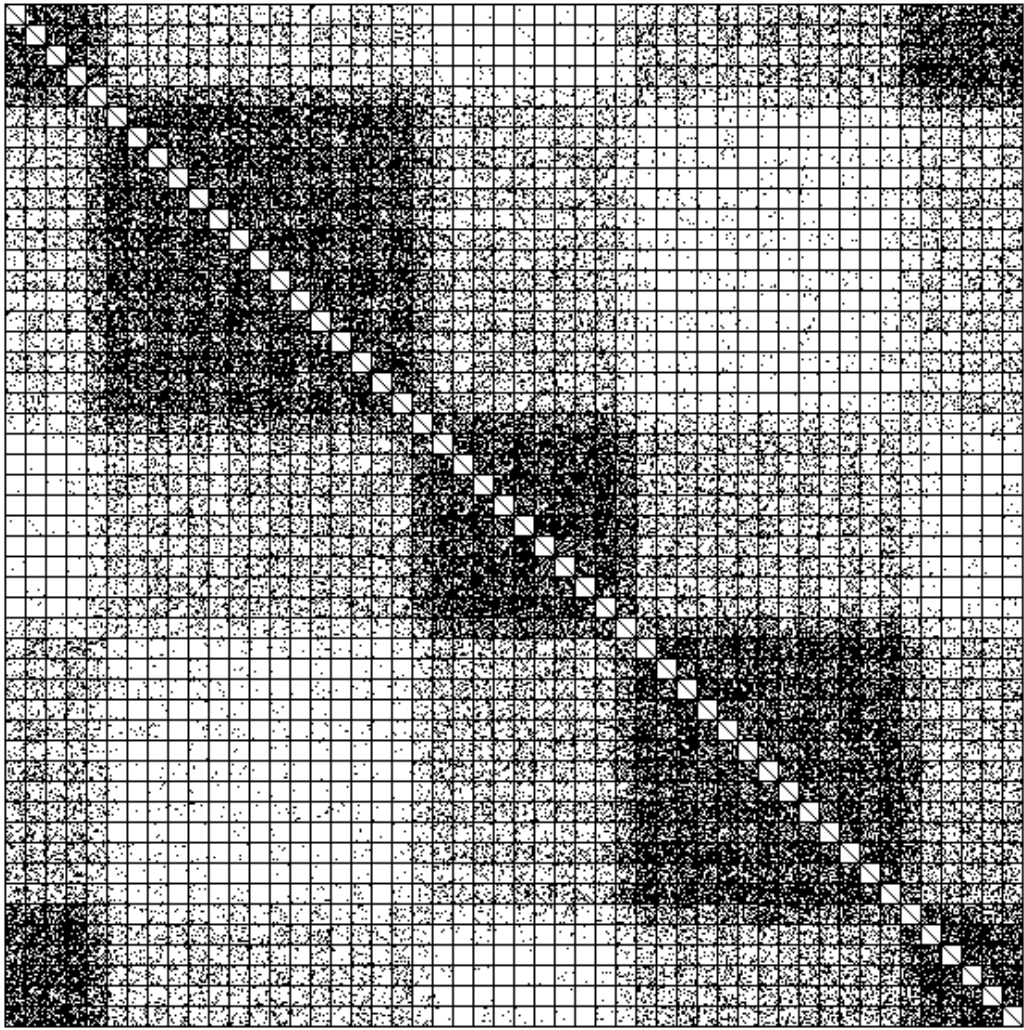


Fig. 12c

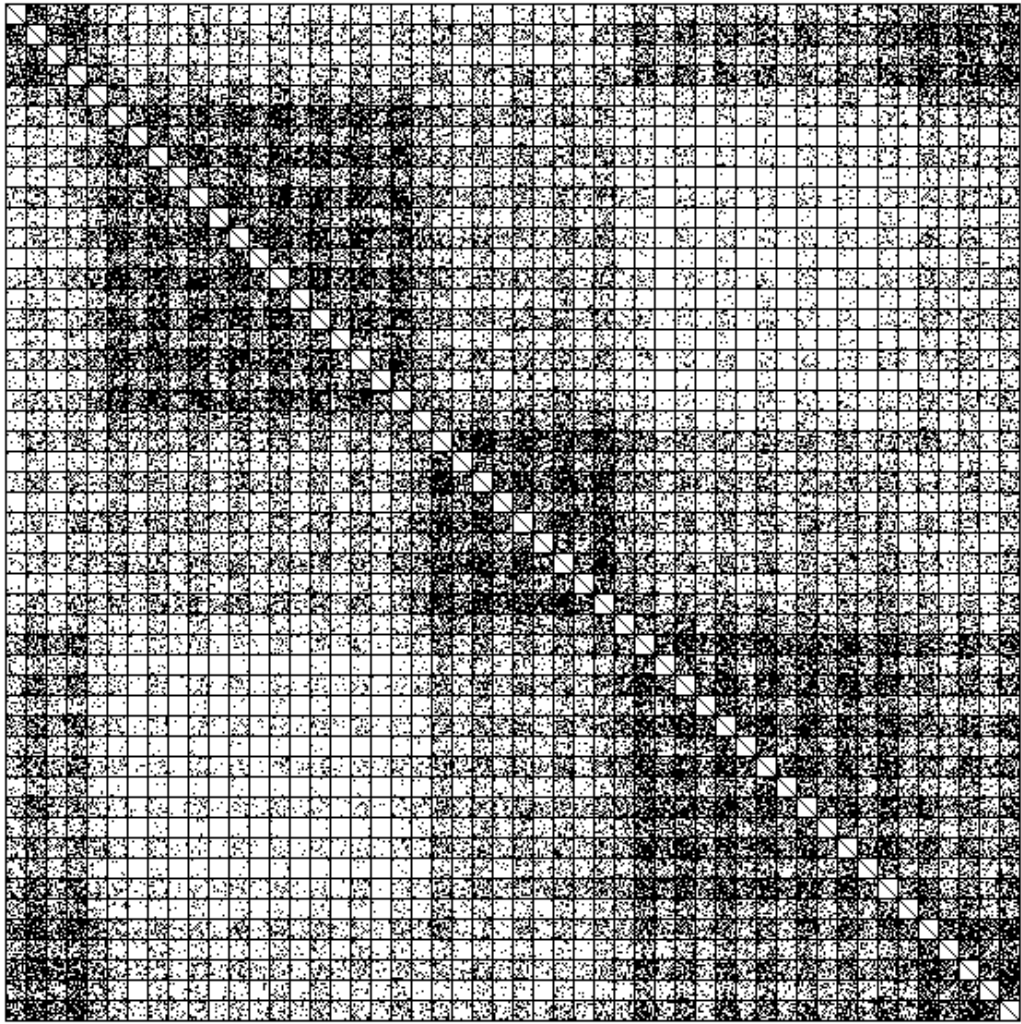


Fig. 12d



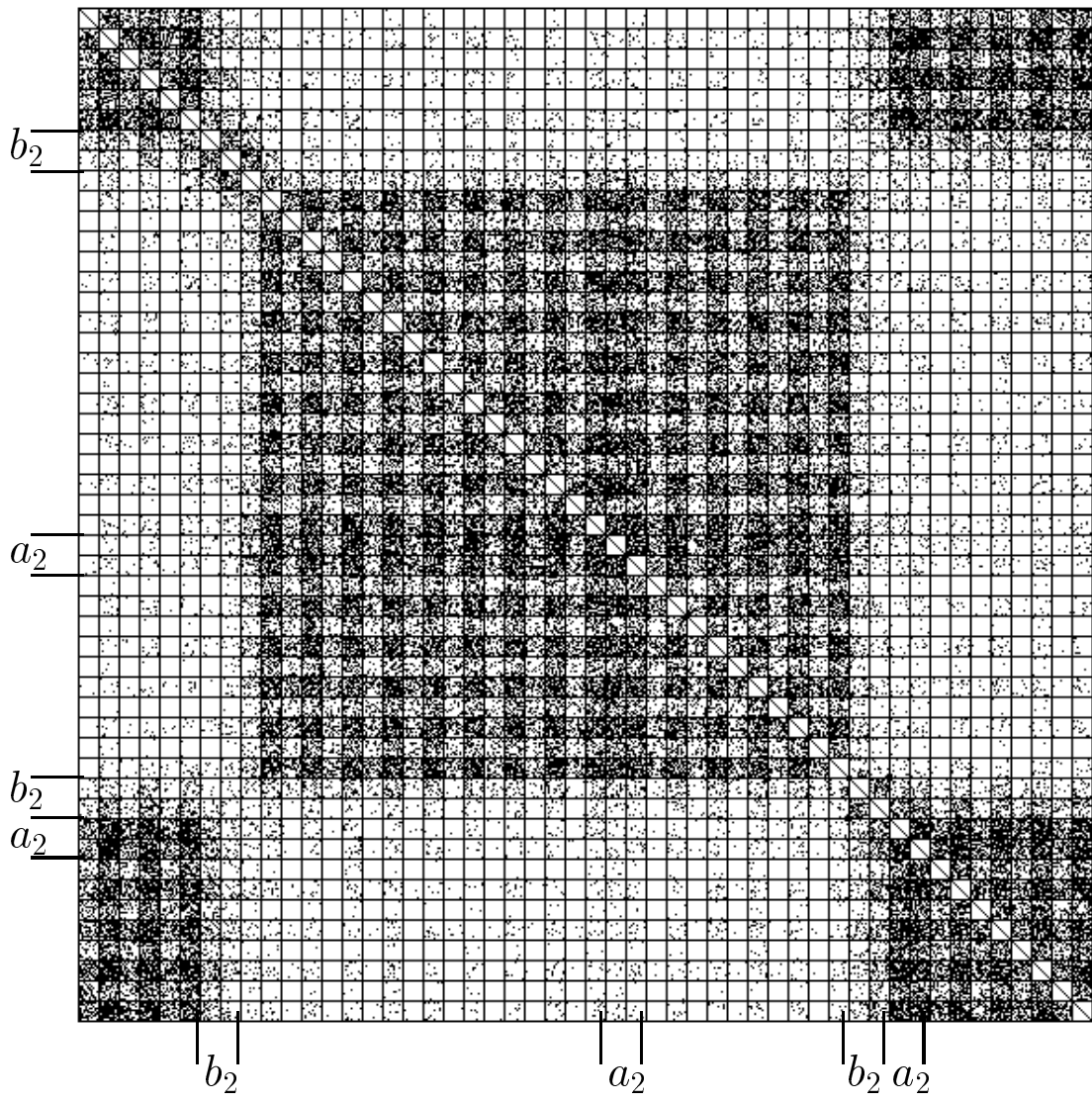


Fig. 13